

1 USP28 enables oncogenic transformation of respiratory cells and its inhibition  
2 potentiates molecular therapy targeting mutant EGFR, BRAF and PI3K.

3  
4 Cristian Prieto-Garcia<sup>1,2,3</sup>, Oliver Hartmann<sup>1,2</sup>, Michaela Reissland<sup>1,2</sup>, Fabian  
5 Braun<sup>1,2</sup>, Süleyman Bozkurt<sup>4</sup>, Carmina Fuss<sup>1,2,5</sup>, Christina Schüle-Völk<sup>6</sup>, Alexander  
6 Buchberger<sup>7</sup>, Marco A. Calzado Canale<sup>8,9,10</sup>, Mathias Rosenfeldt<sup>2,11</sup>, Ivan Dikic<sup>3,12</sup>,  
7 Christian Münch<sup>4</sup> & Markus E. Diefenbacher<sup>1,2\*</sup>

8  
9 <sup>1</sup> Protein Stability and Cancer Group, University of Wuerzburg, Department of Biochemistry and  
10 Molecular Biology, Wuerzburg, Germany

11 <sup>2</sup> Mildred Scheel Early Career Center, Wuerzburg, Germany

12 <sup>3</sup> Molecular Signaling Group, Institute of Biochemistry II, Goethe University Frankfurt, Germany

13 <sup>4</sup> Protein quality control, Institute of Biochemistry II, Goethe University Frankfurt, Germany

14 <sup>5</sup> Department of Internal Medicine I, Division of Endocrinology and Diabetes, University Hospital,  
15 University of Wuerzburg, Wuerzburg, Germany

16 <sup>6</sup> Core Unit High-Content Microscopy, Biocenter, University of Wuerzburg, Germany

17 <sup>7</sup> Department of Biochemistry, Biocenter, University of Wuerzburg, 97074 Würzburg, Germany

18 <sup>8</sup> Instituto Maimónides de Investigación Biomédica de Córdoba (IMIBIC), Córdoba, Spain

19 <sup>9</sup> Departamento de Biología Celular, Fisiología e Inmunología, Universidad de Córdoba, Córdoba,  
20 Spain

21 <sup>10</sup> Hospital Universitario Reina Sofía, Córdoba, Spain

22 <sup>11</sup> Institut für Pathologie, Universitaetsklinikum Wuerzburg

23 <sup>12</sup> Buchmann Institute for Molecular Life Sciences, Goethe University Frankfurt, Germany.

24 \*corresponding author

25  
26  
27 **Keywords:** USP28, c-MYC, c-JUN, lung cancer, EGFR, PIK3CA, BRAF, HRAS  
28 Gefitinib, Buparlisib, Vemurafenib.

29  
30 **Financial Support:** C.P.G. and O.H. are supported by the German Cancer Aid via  
31 grant 70112491. M.R. is funded by the DFG-GRK 2243 and IZKF B335. M.E.D. is  
32 funded by the German Israeli Foundation grant 1431.

33  
34 **\*Corresponding Author:** Dr. Markus E. Diefenbacher. Lehrstuhl für Biochemie und  
35 Molekularbiologie, Biozentrum, Am Hubland, Würzburg, 97074, Germany. Phone:  
36 0931 31-88167; Fax: 0931 31-84113; E-mail: markus.diefenbacher@uni-  
37 wuerzburg.de

38  
39 **Conflict of Interest:** The authors declare no potential conflicts of interest.

40  
41  
42  
43  
44  
45  
46

47

48 **Abstract**

49 Oncogenic transformation of lung epithelial cells is a multi-step process, frequently  
50 starting with the inactivation of tumor suppressors and subsequent activating  
51 mutations in proto-oncogenes, such as members of the PI3K or MAPK family. Cells  
52 undergoing transformation have to adjust to changes, such as metabolic  
53 requirements. This is achieved, in part, by modulating the protein abundance of  
54 transcription factors, which manifest these adjustments. Here, we report that the  
55 deubiquitylase USP28 enables oncogenic reprogramming by regulating the protein  
56 abundance of proto-oncogenes, such as c-JUN, c-MYC, NOTCH and  $\Delta$ NP63, at  
57 early stages of malignant transformation. USP28 is increased in cancer compared to  
58 normal cells due to a feed-forward loop, driven by increased amounts of oncogenic  
59 transcription factors, such as c-MYC and c-JUN. Irrespective of oncogenic driver,  
60 interference with USP28 abundance or activity suppresses growth and survival of  
61 transformed lung cells. Furthermore, inhibition of USP28 via a small molecule  
62 inhibitor reset the proteome of transformed cells towards a 'pre-malignant' state, and  
63 its inhibition cooperated with clinically established compounds used to target  
64 EGFR<sup>L858R</sup>, BRAF<sup>V600E</sup> or PI3K<sup>H1047R</sup> driven tumor cells. Targeting USP28 protein  
65 abundance already at an early stage via inhibition of its activity therefore is a feasible  
66 strategy for the treatment of early stage lung tumours and the observed synergism  
67 with current standard of care inhibitors holds the potential for improved targeting of  
68 established tumors.

69

70

## 71 Introduction

72

73 In the past decade, with the advent of targeted therapy, great advancements towards  
74 the treatment of progressed Non-Small Cell Lung Cancer (NSCLC) in distinct patient  
75 cohorts were achieved(1), while patients with early disease do not benefit from these  
76 new treatments(2, 3). For this cohort, the curative treatment, still today, is the  
77 surgical resection of a lung lobe. This is a severe procedure, inflicting major damage,  
78 requires an extended recovery time and can result in therapy induced mortality(4, 5).  
79 Furthermore, therapy failure in late stage tumours by establishment of treatment  
80 escape mechanisms is a common observation in NSCLC, significantly affecting  
81 patient survival(6, 7). Overall, survival rates have only marginally improved and most  
82 patients still succumb to the disease(1).

83

84 Therefore, targeting of common essential pathways and exploiting tumour intrinsic  
85 vulnerabilities holds the potential to not only improve current treatment for late stage,  
86 but also for early stage patients. One central cellular component tumour cells alter  
87 during oncogenic transformation is the ubiquitin proteasome system (UPS)(8, 9). The  
88 dysregulation of the UPS is a prerequisite for tumor cells to tolerate increased  
89 proliferation, metabolic changes, immune evasion and proteostatic stress  
90 management(10). All these processes are 'hallmarks of cancer' and therefore  
91 significantly contribute to disease progression, therapy failure and shorted survival.  
92 Therefore, cancer cells, when compared to non-transformed cells, are dependent on  
93 the ubiquitin system(11, 12). As a consequence, tumour cells develop exploitable  
94 dependencies towards the expression and abundance of discreet members of the  
95 UPS<sup>12</sup>.

96

97 Despite the prominent involvement of the UPS in cancer, our understanding of how  
98 tumour cells alter the UPS system very early in transformation is rather limited(12).  
99 The identification of essential and druggable key-players within this class of enzymes  
100 has the potential to hold novel therapeutic strategies. Deubiquitinating enzymes are  
101 such a therapeutically promising class of enzymes, as individual members can be  
102 targeted by small molecule inhibitors(13-15).

103

104 In this study, we report that the deubiquitylase USP28 presents a UPS enzyme,  
105 which is commonly upregulated during early stages of oncogenic transformation in  
106 lung cancer. Irrespective of oncogenic driver, tumour cells upregulate USP28, which  
107 stabilizes proto-oncogenes, such as c-MYC, c-JUN or NOTCH. Tumour cells are  
108 addicted to USP28 to allow oncogenic transformation and its inhibition via the small  
109 molecule inhibitor AZ1(16) partially reverts the oncogenic transformation. Finally,  
110 combining USP28 targeting with targeted therapy against commonly found  
111 oncogenic drivers potentiates treatment responses, at least *in cellulo*, indicating that  
112 the UPS system, exemplified by USP28, is a promising target structure for lung  
113 cancer.

114

115

## 116 **Materials and Methods**

117

### 118 **Cell lines**

119

120 Human basal bronchial epithelial BEAS-2B cells were originally transformed with  
121 SV40-large-T-antigen (Reddel et al., 1988). The cell line BEAS-2B was a kind gift of  
122 Prof. Marco A. Calzado Canales (Universidad de Córdoba, Hospital Reina Sofia,  
123 Córdoba, Spain). BEAS-2B Oncogenic cells were generated upon retroviral infection  
124 of BEAS-2B DIF with the next plasmids: EGFR (addgene number: #11011), EGFR  
125 L858R (addgene number: #11012), pBabe puro HA PIK3CA (addgene number:  
126 #12522), pBabe puro HA PIK3CA H1047R (addgene number: #12524), pBabe puro  
127 HA PIK3CA E545K (addgene number: #12525), pBabe puro HRAS G12D (HRAS  
128 G12D was cloned into pBabe puro in our lab) and pBabe puro BRAF V600E  
129 (addgene number: #15269). The plasmids EGFR and EGFR L858R were a gift from  
130 Matthew Meyerson (Greulich H, Chen TH et al. 2005). pBabe puro HA PIK3CA  
131 H1047R, HA PIK3CA E545K, HA PIK3CA were a gift from Jean Zhao (Zhao JJ, Liu  
132 Z, Wang L et al. 2005). pBabe Puro BRAF V600E was a gift from William Hah  
133 (Boehm et al Cell. 2007) For virus production HEK293-T cells were used. Cell lines  
134 used in this publication are listed in the supplementary table called: Consumables  
135 and resources.

136

### 137 **Tissue culture reagents and drugs.**

138

139 Cells were plated on Greiner dishes and incubated at 37 °C, 95 % relative humidity  
140 and 5 % CO<sub>2</sub> in a cell incubator for optimal growth conditions. DIF BEAS-2B,  
141 oncogenic BEAS-2B and HEK-293T cells were cultured in DMEM (Gibco)  
142 supplemented with 10% fetal bovine serum (FCS)/ 1% Pen-Strep. UD cells were  
143 cultured in LHC-9 (Gibco) supplemented with 1% Pen/Strep. To cultivate UD BEAS-  
144 2B cells, the dishes were pre-coated with pre-coating solution composed by: 0.03%  
145 Collagen (in 0.1 M acetic acid), 0.01% Fibronectin and 0.001% BSA. UD cells were  
146 supplemented with 10% FCS to induce pre-oncogenic differentiation. Cells were  
147 routinely tested for mycoplasma via PCR. The reagents and drugs were dissolved in  
148 Dimethyl sulfoxide (DMSO). AZ1, Gefitinib, Buparlisib and Vemurafenib were  
149 purchased from Selleckchem. Drugs and reagents are listed in the supplementary  
150 table called: Consumables and resources.

151

### 152 **AAV, Retrovirus and Lentivirus production and purification**

153

154 Adeno-associated viruses (AAVs) were generated and packaged in HEK293-T cells  
155 seeded in 15-cm cell culture dishes (60-70% confluence). Cells were transfected  
156 with the plasmid of interest (10 µg), pHelper (15 µg) and pAAV-DJ (10 µg) using PEI  
157 in ratio 2:1 (70 µg). After 96 hours, AAV Virus isolation from cells was performed as  
158 previously described (17). For Retrovirus production, HEK293 cells (70%



159 confluence) were transfected with the babe plasmid of interest (15 µg), pUMVC (10  
160 µg) and VSV-G (10 µg) using PEI (70 µg). After 96 H, the medium containing retrovirus  
161 was filtered (0.45 µM) and stored at -80°C. For Lentivirus production, HEK293 cells  
162 (70% confluence) were transfected with the plasmid of interest (15 µg), pPAX (10  
163 µg) and pPMD2 (10 µg) using PEI (70 µg). After 96 H, the medium containing  
164 lentivirus was filtered (0.45 µM) and stored at -80°C.

165

## 166 **In vitro DNA transfection and infection**

167

168 DNA transfection was performed exposing 60% confluence BEAS-2B cells plated in  
169 a 6-well cell culture dish to a mix of 2.5µg plasmid of interest, 200µl DMEM free  
170 serum and 5µl PEI (1:2 ratio). Upon 6h incubation at 37°C, 5% CO<sub>2</sub> and 95%  
171 relative humidity, the medium was removed and substituted by DMEM (Gibco)  
172 supplemented with 10% FCS/ 1% Pen-Strep. For viral infection, 10 MOI (multiplicity  
173 of infection) of Retroviruses (LVs) were added to normal medium of the cells in the  
174 presence of polybrene (5µg/ml). Cells exposed to the viruses were incubated at  
175 37°C, 5% CO<sub>2</sub> and 95% relative humidity for 4 days. The infected cells were  
176 identified and selected by exposure to 2.5µg/ml Puromycin for 72h.

177

## 178 **RT-PCR**

179

180 RNA was isolated with Peq GOLD Trifast (Peqlab), as indicated in the  
181 manufacturer's instructions. RNA was reverse transcribed into cDNA using random  
182 hexanucleotide primers and M-MLV enzyme (Promega). Quantitative RT-PCR was  
183 performed with SYBR Green mix (ABgene) on the instrument "Step One Realtime  
184 Cycler" (ABgene) The RT-PCR program employed in this research is the following:  
185 95°C for 15 min., 40x [95°C for 15 sec., 60°C for 20 sec. and 72°C for 15 sec.], 95°C  
186 for 15 sec. and 60°C for 60 sec. Relative expression was generally calculated with  
187  $\Delta\Delta C_t$  relative quantification method. Melt curve was performed for all primers. For  
188 visualization purposes, Excel (Microsoft) and Affinity Designer were used as  
189 bioinformatic tools. Primers used for this publication are listed in the supplementary  
190 table called: Consumables and resources.

191

## 192 **Plasmids, sgRNA and shRNA Design**

193

194 sgRNAs were designed using the CRISPR online tool: [https://zlab.bio/guide-design-](https://zlab.bio/guide-design-resources)  
195 [resources](https://zlab.bio/guide-design-resources)). shRNAs were designed using SPLASH-algorithm:  
196 <http://splashrna.mskcc.org/>) or RNAi Consortium/Broad Institute:  
197 [www.broadinstitute.org/rnai-consortium/rnai-consortium-shrna-library](http://www.broadinstitute.org/rnai-consortium/rnai-consortium-shrna-library).

198 Oligonucleotides used in this publication are listed in the supplementary table called:  
199 Consumables and resources.

200

## 201 **Operetta analysis, Immunofluorescence, cell viability, Bliss synergy and GI50**

202

203 Number of cells was quantified using Operetta High-Content Imaging System  
204 (PerkinElmer) (number of DAPI positive cells) or Invitrogen Countess II FL (number  
205 of cells after trypsinization) upon indicated treatments. For the Operetta High-  
206 Content Imaging System, cells were seeded in 384-well plates at equal density and  
207 exposed to indicated treatments. Then, cells were fixed using 4% PFA for 10  
208 minutes and then, permeabilized using 0.5% Triton X-100 in PBS for 5 minutes. For IF,  
209 primary antibodies (1/100) were incubated ON at 4°C, followed by subsequent  
210 incubation with the secondary antibody (1/300) for 1 hour at room temperature. After  
211 antibody exposure, samples were washed twice with PBS. Before quantification cells  
212 were stained with DAPI (ThermoFisher). For the quantification of dead cells, 1 µg/ml  
213 PI was added to the cell medium of live cells for 20 minutes upon indicated  
214 treatments. For quantification of dead cells, 1 µg/ml PI (Sigma Aldrich) was added to  
215 the cell medium of live cells for 20 minutes upon indicated treatments. For  
216 quantification of proliferative cells, samples were subjected to KI67 (Santa Cruz ab:  
217 sc-23900; 1/100) staining by IF before imaging. Number of dead, proliferative and  
218 total cells were determined counting the number of positive nucleus for PI, KI67 or  
219 DAPI with the Harmony Software (Perkin Elmer). Bliss synergy was calculated using  
220 the total number of cells upon indicated treatments. For calculation of synergy,  
221 Combenefit software was previously described (Di Veroli GY et al 2016). GI<sub>50</sub> was  
222 generated using the online tool: [www.aatbio.com](http://www.aatbio.com). For Crystal violet cell viability, cells  
223 were stained with 0.5% Crystal violet and analyzed using ImageJ software (staining  
224 intensity is between 0 to 255). For visualization purposes, Excel (Microsoft) and  
225 Affinity Designer were used as bioinformatic tools. Antibodies used in this publication  
226 are listed in the supplementary table called: Consumables and resources.

227

## 228 **Immunoblot**

229

230 Cells were lysed in RIPA lysis buffer (20 mM Tris-HCl pH 7.5, 150 mM NaCl, 1 mM  
231 Na<sup>2</sup>EDTA, 1 mM EGTA, 1% NP-40 and 1% sodium deoxycholate), supplemented  
232 with proteinase inhibitor (1/100) via sonication with Branson Sonifier 250 (duty cycle  
233 at 20% and output control set on level 2; 10 sonication / 1 minute cycles per sample).  
234 50 µg protein was boiled in 5x Laemmli buffer (312.5 mM Tris-HCl pH 6.8, 500 mM  
235 DTT, 0.0001% Bromophenol blue, 10% SDS and 50% Glycerol) for 5 min and  
236 separated on 10% Tris-gels in Running buffer (1.25 M Tris base, 1.25 M glycine and  
237 1% SDS). After separation, protein was transferred to Polyvinylidene difluoride  
238 membranes (Immobilon-FL) in Transfer Buffer (25 mM Tris base, 192 mM glycine and  
239 20% methanol). Membrane was exposed to blocking buffer (0.1% casein, 0.2x PBS  
240 and 0.1% Tween20) for 45-60 min at room temperature (RT). Then, membranes  
241 were incubated with primary antibody (1/1000) in a buffer composed by 0.1% casein,  
242 0.2x PBS and 0.1% Tween20) for 6h at room temperature (RT). Membrane was  
243 incubated with indicated secondary Antibody (1/10000) in a buffer composed by  
244 0.1% casein, 0.2x PBS, 0.1% Tween20 and 0.01% SDS for 1h at RT. Membranes  
245 were recorded in Odyssey® CLx Imaging System, and analysed using Image Studio

246 software (Licor Sciences). Antibodies used in this publication are listed in the  
247 supplementary table called: Consumables and resources.

248

### 249 **Ubiquitin Suicide Probe/Warhead DUB activity assays**

250

251 Cells were resuspended in HR-buffer (50 mM Tris-HCl pH 7.4, 5 mM MgCl<sub>2</sub>, 250  
252 mM Sucrose, 0,1 % NP-40), supplemented with Protease-Inhibitor. Lysis was  
253 performed by three freeze-thaw cycles. 25 µg of cell lysate were transferred to a new  
254 eppendorf tube and 3 µL of a 1:1:1 mixture of Ub-VME, Ub-VS, Ub-PA suicide-  
255 probes (UbiQ) resuspended in 50 mM NaOAc, 5 % DMSO were added to the  
256 mixture. In order to adjust the pH, 50 mM NaOH was added. Then, samples were  
257 mixed and incubated for 1 hour at 37°C shaking. After addition of Laemmli-buffer,  
258 samples were boiled for 5 min and applied to immunoblot was performed.

259

### 260 **Human lung cancer samples**

261

262 Human samples were obtained from Pathology Department Córdoba (Spain),  
263 Pathology Department University Hospital Würzburg (Germany) and U.S. Biomax  
264 (lung microarray slides; slide LC2083). Informed consent was obtained from all  
265 patients. Experiments were in agreement to the principles set out in the WMA  
266 Declaration of Helsinki and the Department of Health and Human Services Belmont  
267 Report. Samples are approved under ethical approval license decret 439/2010  
268 (Hospital Universitario Reina Sofía) and Ethics approval 17/01/2006 (University  
269 Hospital Würzburg).

270

### 271 **Analysis of human publicly available datasets**

272

273 Oncoprints were generated using cBioportal online tool. Briefly, Oncoprints  
274 generates graphical representations of genomic alterations, somatic mutations, copy  
275 number alterations and mRNA expression changes. Graphical representations of  
276 somatic mutations were performed using the online tool Cbioportal. TCGA data was  
277 used for the different analysis. Correlation analysis and USP28 expression in  
278 different subtypes of ADC and SCC lung tumors were obtained using GEPIA's  
279 software (Tang Z. et al. 2017). For GEPIA gene expression. the differential analysis  
280 was based on: "TCGA tumors vs (TCGA normal)", whereas the expression data  
281 were log<sub>2</sub>(TPM+1) transformed and the log<sub>2</sub>FC was defined as median(tumor) –  
282 median(normal). p-values were calculated with a one-way ANOVA comparing tumor  
283 with normal tissue.

284

285 The online tool KMplot (Nagy et al. 2018) was used to analyze different types of  
286 survivals and generate Kaplan-meier curves based on gene expression data from  
287 microarrays obtained from GEO, caBIG and TCGA. Using the KM plotter online tool,  
288 patients were split using the option 'Auto select best cutoff' in high or low USP28  
289 gene expression groups. P values for log rank tests of the Kaplan–Meier curves

290 were calculated with the online tool KM plotter. Depmap (version 2020) was used to  
291 analyze and visualize Pearson correlation between the genetic expression of USP28  
292 and BRAF/AKT2 in cancer cell lines. p-value and linear regression was calculated by  
293 the online tool depmap. <https://depmap.org/>

294

295 Survival of patients with KRAS, EGFR, PIK3CA and BRAF mutated tumors was  
296 analysed using the online tool UCSC Xena (Goldman et al. 2020). USP28 gene  
297 expression of lung cancer samples (including KRAS, EGFR, PIK3CA and BRAF  
298 mutated samples) were obtained from TCGA dataset. Gene expression was  
299 downloaded as log<sub>2</sub> (norm\_count+1). Samples were divided in two groups  
300 (High/Low USP28) based on USP28 expression. Expression of USP28 was defined  
301 as high when the respective expression levels were higher than the median  
302 expression levels of the analysed dataset. Expression of USP28 was defined as low  
303 when the respective expression levels were lower than the median expression levels  
304 of the analysed dataset. Box plots using TCGA and GTEx data were generated  
305 using the online tool BoxPlotR (Spitzer M. et al. 2014) In box plots, the centre line  
306 reflects the median and the upper and lower box limits indicate the first and third  
307 quartiles. Whiskers extend 1.5× the IQR. For BoxplotR, the data previously  
308 download from UCSC Xena was used to generate the graphics, p-values were  
309 calculated using two-tailed t-test. Softwares used for this publication are listed in the  
310 supplementary table called: Consumables and resources.

311

### 312 **Animal Experiments and histology.**

313

314 All *in vivo* experiments were approved by the Regierung Unterfranken and the ethics  
315 committee under the license numbers 2532-2-362, 2532-2-367, 2532-2-374 and  
316 2532-2-1003. All animals are housed in standard cages in pathogen-free facilities on  
317 a 12h light/dark cycle with *ad libitum* access to food and water. FELASA2014  
318 guidelines were followed for animal maintenance. Veterinarians supervise the  
319 welfare of the animals every day. In presence of pain, stress or suffering, mice were  
320 immediately euthanized by cervical dislocation upon Isoflurane anesthesia. The  
321 mouse strains used for this publication are listed in the supplementary table called:  
322 Consumables and resources.

323

324 Adult mice were anesthetized with Isoflurane and intratracheally intubated with 50 µl  
325 AAV virus ( $3 \times 10^7$  PFU) as previously described (17). Animals were sacrificed by  
326 cervical dislocation and lungs were fixed using 5% NBF. For IHC and H&E, slides  
327 were de-paraffinized and rehydrated following the previously reported protocol (17).  
328 Briefly, IHC slides were subjected to epitope retrieval and blocked in 3% BSA at RT  
329 for 1h. Antibody manufacturer instructions were followed for every antibody. But in  
330 general, primary antibodies (diluted in 1% BSA) were incubated ON at 4°C followed  
331 by three washes with PBS and the subsequent incubation with the DAB secondary  
332 antibody for 1 hour at RT. Then, slides were washed twice with 1xPBS for 5 min and  
333 stained with the DAB staining solution in 1xPBS. Upon DAB staining, slides were

334 counteracted with hematoxylin and washed three times with 1x PBS for 5 min.  
335 Slides were mounted with 200  $\mu$ l of Mowiol® 40-88 covered up by a glass coverslip.  
336 IHC slides were recorded using Panoramic DESK scanner or using  
337 FSX100 microscopy system (Olympus) and analysed using Case Viewer software  
338 (3DHISTECH), QuPath software and ImageJ. IF samples were recorded using  
339 FSX100 microscopy system (Olympus). Antibodies used in this publication are listed  
340 in the supplementary table called: Consumables and resources.

341

### 342 **Organotypic lung tumor slice cultures ex vivo**

343

344 Lung tumors developed upon endotracheal transplantation of KPL cells as previously  
345 described (17) or WT lung tissue from WT C57BL6/J-Rosa26 Sor-CAGG-Cas9-  
346 IRES-eGFP animals were explanted and sectioned in slices using the vibratome. Ex  
347 vivo slices were relocated in cell culture dishes and maintained in standard cell  
348 culture medium (DMEM, 10% FCS) and conditions (37°C, 5% CO<sub>2</sub> and 95% relative  
349 humidity).

350

### 351 **Sample preparation for mass spectrometry**

352

353 The sample preparation was performed as described previously. In brief, lysates  
354 were precipitated by methanol/chloroform and proteins resuspended in 8 M Urea/10  
355 mM EPPS pH 8.2. Concentration of proteins was determined by Bradford assay and  
356 100  $\mu$ g of protein per samples was used for digestion. For digestion, the samples  
357 were diluted to 1 M Urea with 10mM EPPS pH 8.2 and incubated overnight with 1:50  
358 LysC (Wako Chemicals) and 1:100 Sequencing grade trypsin (Promega). Digests  
359 were acidified using TFA and tryptic peptides were purified by tC18 SepPak (50 mg,  
360 Waters). 10  $\mu$ g peptides per sample were TMT labelled and the mixing was  
361 normalized after a single injection measurement by LC-MS/MS to equimolar ratios  
362 for each channel. A bridge channel was prepared by pooling 3  $\mu$ g from all 24  
363 samples which were TMT-labeled together and split into two 10  $\mu$ g samples for each  
364 plex, 130  $\mu$ g of pooled peptides were dried for High pH Reversed-phase  
365 fractionation.

366

### 367 **High pH reversed-phase fractionation**

368

369 Labeled peptide samples were pooled, fractionated into 8 fractions using the High  
370 pH Reversed-Phase Peptide Fractionation Kit (ThermoFisher Scientific 84868)  
371 according to the manufacturer protocol and dried. Additionally, for label free single  
372 shots, 10  $\mu$ g of peptide is cleaned up with Empore C18 stage tipping and dried right  
373 away for shooting.

374

### 375 **LC-MS<sup>3</sup> proteomics**

376



377 All mass spectrometry data was acquired in centroid mode on an Orbitrap Fusion  
378 Lumos mass spectrometer hyphenated to an easy-nLC 1200 nano HPLC system  
379 using a nanoFlex ion source (ThermoFisher Scientific) applying a spray voltage of  
380 2.6 kV with the transfer tube heated to 300°C and a funnel RF of 30%. Internal mass  
381 calibration was enabled (lock mass 445.12003 m/z). Peptides were separated on a  
382 self-made, 32 cm long, 75µm ID fused-silica column, packed in house with 1.9 µm  
383 C18 particles (ReproSil-Pur, Dr. Maisch) and heated to 50°C using an integrated  
384 column oven (Sonation). HPLC solvents consisted of 0.1% Formic acid in water  
385 (Buffer A) and 0.1% Formic acid, 80% acetonitrile in water (Buffer B).

386 For total proteome analysis, a synchronous precursor selection (SPS) multi-notch  
387 MS3 method was used in order to minimize ratio compression as previously  
388 described (McAlister et al., 2014). Individual peptide fractions were eluted by a non-  
389 linear gradient from 3 to 60% B over 150 minutes followed by a step-wise increase to  
390 95% B in 6 minutes which was held for another 9 minutes. Full scan MS spectra  
391 (350-1400 m/z) were acquired with a resolution of 120,000 at m/z 200, maximum  
392 injection time of 100 ms and AGC target value of  $4 \times 10^5$ . The most intense  
393 precursors with a charge state between 2 and 6 per full scan were selected for  
394 fragmentation within 3 s cycle time and isolated with a quadrupole isolation window  
395 of 0.7 Th. MS2 scans were performed in the Ion trap (Turbo) using a maximum  
396 injection time of 50ms, AGC target value of  $15 \times 10^4$  and fragmented using CID with  
397 a normalized collision energy (NCE) of 35%. SPS-MS3 scans for quantification were  
398 performed on the 10 most intense MS2 fragment ions with an isolation window of 1.2  
399 Th (MS) and 2 m/z (MS2). Ions were fragmented using HCD with an NCE of 65%  
400 and analyzed in the Orbitrap with a resolution of 50,000 at m/z 200, scan range of  
401 110-500 m/z, AGC target value of  $1.5 \times 10^5$  and a maximum injection time of 150ms.  
402 Repeated sequencing of already acquired precursors was limited by setting a  
403 dynamic exclusion of 60 seconds and 7 ppm and advanced peak determination was  
404 deactivated.

#### 405 **Proteomics analysis**

406 Proteomics raw files were processed using proteome discoverer 2.2 (ThermoFisher).  
407 Spectra were recalibrated using the Homo sapiens SwissProt database (2020-03-12)  
408 and TMTpro (+304.207 Da) as static modification at N-terminus and Lysines,  
409 together with Carbamidomethyl at cysteine residues. Spectra were searched against  
410 human database and common contaminants using Sequest HT with oxidation (M) as  
411 dynamic modification together with methionine-loss + acetylation and acetylation at  
412 the protein terminus. TMTpro (N-term, K) and carbamidomethyl were set as fixed  
413 modifications. Quantifications of spectra were rejected if average S/N values were  
414 below 5 across all channels and/or isolation interference exceeded 50%. Protein  
415 abundances were calculated by summing all peptide quantifications for each protein.  
416 Two mixing two plexes, a bridge channel was used additionally. Internal reference  
417 scaling (IRS) normalization was performed to obtain proteomics data set across two  
418 plexes.  
419



420 Reactome analysis was performed with PANTHER using the “Statistical  
421 overrepresentation test” tool with default settings. For Reactome analysis and Violin  
422 plots, the common proteins significantly dysregulated in EGFR L858R, BRAF V600E  
423 and PIK3CA H1047R BEAS-2B respect to DIF. BEAS-2B cells were selected.  
424 Proteins were considered significantly downregulated when  $p\text{-value} < 0.05$ . Z-score  
425 heatmap visualization was performed using Morpheus (Broad Institute). The  
426 maximum and minimal Z-score per row used in heatmaps was calculated using  
427 Morpheus (Broad Institute). Volcano plots were generating using the software  
428 Instant Clue (Nolte et al. 2018). Venn Diagrams were performed using the online  
429 tool: <http://bioinformatics.psb.ugent.be/webtools/Venn/>. PCA analysis was performed  
430 using the online tool CLUSTVIS (Tauno Metsalu and Jaak Vilo 2015). Violin plots  
431 were generated using the online tool BoxPlotR (Spitzer M. et al. 2014). For  
432 visualization purposes, Excel (Microsoft) and Affinity Designer were used as  
433 bioinformatic tools.

434

#### 435 **Data and Software availability**

436 Proteomic data is available at PRIDE.

437

#### 438 **Contact for reagent and resource sharing**

439 Further information and requests for resources and reagents should be directed to  
440 and will be fulfilled by the Lead Contact, Markus E. Diefenbacher  
441 ([markus.diefenbacher@uni-wuerzburg.de](mailto:markus.diefenbacher@uni-wuerzburg.de)).

442

#### 443 **Results**

444

#### 445 ***USP28 is expressed in human ‘cell-of-origin’ for NSCLC and upregulated*** 446 ***irrespective of lung tumour subtype***

447

448 Previous work has identified the ‘cell-of-origin’ for NSCLC, in particular  
449 adenocarcinoma (BADJ (SPC<sup>+</sup>/CC10<sup>+</sup>) and AT2 (SPC<sup>+</sup>) pulmonary cells)(18, 19),  
450 while squamous cell carcinomas, one of the most mutated tumour entities,  
451 demonstrated a rather high degree of plasticity and flexibility regarding the required  
452 cell of origin(20). Here, the genetic driver combination was the determining  
453 factor(21).

454

455 We previously observed that genetic loss of USP28 affected tumor burden in a  
456 murine *in vivo* NSCLC model(22). To investigate whether this could be attributed to  
457 the expression of USP28 in the stem cell/cell of origin compartment of NSCLC, we  
458 performed immunohistochemistry against USP28 in human lung tissue samples.  
459 High USP28 expression was detectable in the tracheal basal cells (triangular-like  
460 shape), BADJ and AT2 cells, the ‘cells-of-origin’ for NSCLC (Figure 1A and 1B).  
461 Next, we were intrigued if USP28 expression is altered relative to tumour type and/or  
462 grade. To address this question, we analysed publicly available gene expression

463 datasets of NSCLC patients (Figure 1C). *USP28* was found to be upregulated  
464 already at an early stage in lung cancer, when compared to wild type tissue (Figure  
465 1C). Furthermore, *USP28* upregulation is a common feature of tumour cells,  
466 irrespective of histological or molecular tumour subtype (Figure 1C, S1A and S1B).  
467 This was further validated by immunostaining of non-transformed versus tumour  
468 samples from NSCLC patients, where a significant increase in *USP28* protein  
469 abundance was detected already at low grade stages for lung ADC and SCC (Figure  
470 1D and 1E).

471  
472 Analysing survival data and correlating *USP28* expression to tumour stages it  
473 became clear that, especially at early stages, *USP28*<sup>high</sup> expressing tumours  
474 significantly correlated with an overall shortened survival (Figure 1F), and this  
475 observation was independent of tumour subtype (Figure 1G).

476  
477 These data indicated that *USP28* is upregulated upon oncogenic transformation and  
478 that upregulation appears to be an early event in the tumorigenesis of lung and holds  
479 prognostic value.

480  
481 ***USP28 is expressed in murine lung stem cells and required to establish***  
482 ***oncogenic transformation in vivo.***

483  
484 To investigate that *USP28* is required for NSCLC induction and its upregulation  
485 occurs at early stages, we utilised CRISPR/Cas9 genetic engineering mouse models  
486 of NSCLC(22, 23).

487  
488 To this end, we analysed the expression pattern of *Usp28* by immunohistochemistry  
489 in wild-type, non-transformed lungs (Figure 2A). We observed that *USP28* showed a  
490 comparable expression to human samples (Figure 2A and Figure 1B). Overall *Usp28*  
491 expression was elevated in putative stem cells, when compared to  
492 surrounding/neighbouring differentiated cells (Figure 2A).

493  
494 Next, we wondered if the transcriptional upregulation of *USP28* already occurs at  
495 point of transformation. To address this question, we used an *ex vivo* organotypic  
496 lung slice culture model. Here, a non-transformed lung from a C53BL6/J-*Rosa26*<sup>Sor-</sup>  
497 *CAGG-Cas9-IRES-eGFP* mouse(24) was sectioned into 100µm thick sections by using a  
498 vibratome and cultured in standard medium. 24 hours post sectioning, slices were  
499 infected using an adeno-associated virus (AAV) expressing the fluorescent protein  
500 mCherry as infection marker, together with sgRNA to delete *Trp53* and mutate  
501 endogenous *Kras* to *Kras*<sup>G12D</sup> (KP, Figure 2B)(22, 23). As a control vector we used  
502 an mCherry expressing AAV. 7 days post infection, the lung slices were harvested  
503 and mRNA expression of *Usp28* analysed using quantitative PCR (Figure 2B). Here,  
504 *Usp28* expression was significant increased at an early transformative state, when  
505 compared to control virus infected tissue samples.

506

507 Next, we analysed the expression of Usp28 and its substrates c-Myc, c-Jun and  
508 Notch1 at various grades in murine primary tumours, generated by intratracheal  
509 infection with a KP encoding AAV (Figure 2C). Mice were infected at around 8  
510 weeks of age and sacrificed 12 weeks post infection. Tumour grade and type were  
511 assessed using histopathological means (H&E, Ttf-1). Already in low grade primary  
512 tumours Usp28 and its substrates were significantly upregulated when compared to  
513 adjacent, non-transformed lung epithelial tissue (Figure 2D). The increase of Usp28  
514 and the oncogenic transcription factors persisted in higher grade tumours, as seen  
515 by immunohistochemistry (Figure 2D), thereby confirming the observation made in  
516 patients (Figure 1C, 1D, 1E, S1A and S1B).

517  
518 Next, we wondered if the upregulation of Usp28 at an early stage is independent of  
519 the oncogenic driver (Figure S2A and S2B). For that purpose, we generated murine  
520 primary NSCLC using BrafV600E as oncogenic driver. BRAF is genetically altered in  
521 28% of SCC and 25% of ADC lung tumour samples (Figure S2A). To analyse early  
522 stage tumours, mice were sacrificed 4 weeks post infection (Figure S2B). Tumour  
523 grade and type were determined using H&E and immunohistologic stainings against  
524 Ttf1 and PcnA. Already in early stage lung primary tumours, Usp28 was over-  
525 expressed when compared to non-transformed tissue (Figure S2C).

526  
527 Previously we reported that loss of Usp28 affected the induction of lung squamous  
528 cancer, and its genetic loss affected overall tumour burden (22). To investigate if loss  
529 of Usp28 affects tumour induction at an early stage or just reduces proliferation of  
530 transformed cells, next, we infected constitutive Cas9 expressing mice with an AAV  
531 virus containing either an sgRNA to delete *Trp53* and mutate endogenous *Kras* to  
532 *Kras<sup>G12D</sup>* (KP, Figure 2E) or a virus harbouring additional two sgRNA targeting  
533 endogenous Usp28 (KPU, Figure 2E). Mice were sacrificed 4 weeks post infection  
534 and while in KP infected animals' tumour lesions were detectable, in KPU however,  
535 no lesions could be observed (Figure 2F).

536  
537 These data suggest that USP28 is expressed in tumour initiating cells and is  
538 required during early stages of lung cancer transformation independent of tumour  
539 subtype or oncogenic driver.

540  
541 ***USP28 is increased during early transformation in human BEAS-2B***  
542 ***differentiation assay.***

543  
544 As it appears that transcriptional upregulation and increased protein abundance of  
545 USP28 is a required early event in oncogenic transformation, we used a human cell  
546 line system to recapitulate these early events. The immortalised human tracheal cell  
547 line BEAS-2B retains the ability to grow as a progenitor like cell, but in a cell-density  
548 dependent fashion or under the exposure of fetal calf serum (FCS) can terminally  
549 differentiate into a squamous like, pre-oncogenic and highly proliferative cell (Figure  
550 3A)(25, 26). Indeed, culturing these cells under progenitor specific culturing

551 conditions maintained the cells in a 'spindle-like' shape as previously reported  
552 (Figure 3B; undifferentiated BEAS-2B; BEAS-2B<sup>UD</sup>). Upon FCS exposure,  
553 BEAS2B<sup>UD</sup> cells start to alter their morphology and resemble a squamous phenotype  
554 (Figure 3B and 3C; differentiated BEAS-2B; BEAS-2B<sup>DIF</sup>)(25). Furthermore, USP28  
555 protein abundance was increased in BEAS-2B<sup>DIF</sup> when compared BEAS-2B<sup>UD</sup> to by  
556 immunofluorescence and immunoblotting against endogenous USP28 (Figure 3B  
557 and 3C). Not only is USP28 upregulated, but the amount of enzymatically active  
558 USP28 was increased as well, indicated by the amount of USP28 bound to a  
559 ubiquitin suicide probe/warhead (Figure 3D). Upon pre-oncogenic differentiation, the  
560 known USP28 target  $\Delta$ Np63 increased in protein abundance, as shown by  
561 immunoblotting comparing BEAS-2B<sup>DIF</sup> with BEAS-2B<sup>UD</sup> (Figure 3B). To investigate if  
562 the observed differentiation and the consecutive increase in oncoprotein abundance  
563 is USP28 dependent, we exposed BEAS-2B<sup>UD</sup> to FCS (Figure 3E). Upon serum  
564 pulse cells start to differentiate, visualised by brightfield microscopy, and increase  
565 the expression of USP28 and its target  $\Delta$ Np63 (Figure 3E). In order to block USP28,  
566 we made use of the published USP28 inhibitor AZ-1(16, 22). Addition of AZ-1  
567 resulted in the degradation of USP28 and reduction in  $\Delta$ Np63 and cells maintained  
568 an undifferentiated morphology (Figure 3E).

569

570 These data demonstrate that USP28 is upregulated during pre-malignant  
571 transformation and this leads to an increase of USP28 target oncoproteins.

572

573 ***Oncogenic transformation of BEAS-2B<sup>DIF</sup> via EGFR-PI3K-MAPK pathway***  
574 ***upregulate USP28 and accelerates tumour cell growth***

575

576 During the oncogenic transformation process, cells acquire additional alterations,  
577 which are the prerequisite to establish a tumour(27). Using public datasets we  
578 identified that USP28 expression strongly correlates to the expression of common  
579 driver mutations found in NSCLC, encompassing either amplification or mutation of  
580 BRAF, EGFR, PI3K and RAS (Figure 4A and 4B, S3A and S3B). HRAS was the  
581 exemption in RAS family, as no correlation with USP28 was observed in ADC,  
582 however NRAS and KRAS positively correlated with USP28 in ADC human samples  
583 (Figure 4B, S3A and S3B). To test this observation, we *in vitro* retroviral transformed  
584 BEAS-2B<sup>DIF</sup> with various oncogenes (BEAS-2B<sup>ONC</sup>; Figure S3C) and investigated the  
585 effects on USP28 abundance by immunoblotting and RT-PCR. As a control, we used  
586 a virus only encoding Puromycin resistance (Figure S3D and S3E). EGFR WT,  
587 EGFR L858R, HRAS G12D, BRAF V600E, PIK3CA WT, PIK3CA E545A and  
588 PIK3CA H1047R expression was confirmed by immunoblotting and RT-PCR (Figure  
589 S3D and S3E). While USP28 was detectable in control transformed cells, the  
590 expression of oncogenes further increased USP28 levels and mRNA (Figure 4C and  
591 4D). Not only was the DUB increased, but also the USP28 target protein  $\Delta$ Np63,  
592 along with KRT14, a known  $\Delta$ Np63 transcriptional target gene (Figure 4C and  
593 4D)(28). It is noteworthy, that the overexpression of wild type PIK3CA/p110 had little  
594 to no effect on overall protein increase (Figure 4C and 4D). Here, only the mutant

595 variants E545K and H1047R led to an increase in USP28 and  $\Delta$ Np63 (Figure 4C and  
596 4D). More studies are required to elucidate the differences between functional  
597 mutations and amplification of PIK3CA.

598

599 Previous studies reported that USP28 is a direct target of c-JUN and c-MYC (Figure  
600 S4A)(29, 30). Since both proto-oncogenes exert an important role during oncogenic  
601 transformation and are increased upon EGFR-PI3K-MAPK mediated oncogenic  
602 transformation(31), we wondered if the regulation of USP28 in lung cancer depends  
603 on these transcription factors as well. Transient transfection of c-MYC and c-JUN  
604 increased USP28 protein abundance compared to control plasmid transfection in  
605 BEAS-2B cells (Figure S4B). Furthermore, BEAS-2B<sup>DIF</sup> cells showed higher protein  
606 abundance for USP28 and its known substrates c-MYC, c-JUN and NOTCH1 than  
607 BEAS-2B<sup>UD</sup> (Figure S4C) and oncogenic transformation of BEAS-2B<sup>DIF</sup> further  
608 increased USP28, c-MYC, c-JUN and NOTCH1 protein abundance (Figure S4C).

609

610 In summary, c-MYC, c-JUN and NOTCH1 are downstream targets of the PI3K-  
611 MAPK pathways, and establish a feed forward loop in oncogenic transformed cells,  
612 contributing to their increased abundance (Figure S4D). Analysing public datasets  
613 revealed that gene expression of the PI3K-MAPK downstream effectors, AKT2 and  
614 BRAF, positively correlated with USP28 in lung cancer cell lines and in various  
615 tumour entities (Figure S4E). Notably, melanoma and tumours arising in liver, eye  
616 and bone showed weak correlation between USP28 and AKT2-BRAF, and for  
617 thyroid cancer we observed a negative correlation. This tumour type presents a  
618 tumour entity with overall better prognosis and survival(32).

619

620 Next, we wondered if oncogenic transformation of BEAS-2B<sup>DIF</sup> alters cellular growth  
621 responses. To investigate potential effects, we compared growth rates of BEAS-  
622 2B<sup>UD</sup>, BEAS-2B<sup>DIF</sup> and BEAS-2B<sup>ONC</sup> for 4 days (Figure 3E). While the differentiation  
623 already enhanced proliferation and is a consequence of enriched proto-oncogene  
624 abundance (Figure S4C), upon overexpression of oncogenes, irrespective of  
625 oncogenic driver, all generated cell lines demonstrated a significant increase in  
626 proliferation, except overexpression of wild type PIK3CA/p110 (Figure 4E).

627

628 This observation indicates that USP28 is a downstream target of the PI3K-MAPK  
629 pathway (Figure 4F) and is contributing to cellular transformation by stabilising proto-  
630 oncogenes (Figure S4D).

631

### 632 ***Malignant transformation renders tumour cells dependent on USP28***

633

634 As USP28 was upregulated in an oncogene dependent fashion, we wondered if the  
635 increase in USP28 contributes to the pro-proliferative phenotype. The inducible  
636 overexpression of murine USP28 was sufficient to increase the proliferation of  
637 BEAS-2B<sup>DIF</sup> to a comparable extent than PIK3CA mutant cells (Figure 5A).  
638 Conversely, using two independent shRNA sequences to target USP28 expression,



639 irrespective of oncogenic driver, loss of USP28 impaired the proliferation of  
640 transformed cells (Figure 5B). This was further confirmed using the KRAS G12S  
641 mutant lung cancer cell line A549 (Figure S5A). Depletion of USP28 by two  
642 independent shRNA sequences strongly reduced the overall abundance of MYC as  
643 well the proliferation marker PCNA (Figure S5B). As a consequence, A549  
644 proliferation was significantly reduced (Figure S5C). Next, we wondered if the small  
645 molecule inhibitor AZ1, which impairs USP25/28 enzymatic activity, affects  
646 proliferation of oncogenic transformed BEAS-2B. Furthermore, we wanted to  
647 address if the inhibitor shows selectivity towards specific oncogenic drivers. To this  
648 end, BEAS-2B<sup>DIF</sup> and BEAS-2B<sup>ONC</sup> cells were grown in the presence of increasing  
649 concentration of AZ1, followed by calculating the half maximal inhibitory  
650 concentration (IC<sub>50</sub>) by assessing cell numbers. It was revealed that EGFR<sup>L858R</sup>  
651 and BRAF<sup>V600E</sup> transduced BEAS-2B<sup>ONC</sup> cells tolerated ~16µM AZ1, while cells  
652 transformed by PIK3CA<sup>H1047R</sup> required ~20µM (Figure S5D). Given the rather  
653 comparable IC<sub>50</sub> concentrations, we treated BEAS-2B<sup>DIF</sup> and BEAS-2B<sup>ONC</sup> cells with  
654 15 µM AZ1 for 24 hours, followed by immunoblotting against USP28 and its  
655 substrates NOTCH1, c-MYC and c-JUN (Figure 5C). Upon exposure to AZ1, all cell  
656 lines showed a marked reduction in the protein abundance of USP28 and its target  
657 substrates (Figure 5C and 3E). Next, we investigated if AZ1 impairs cell proliferation  
658 or increases cell death in a dose dependent fashion, and if AZ1 affects all cells or is  
659 limited to oncogenic transformed cells (Figure 5D and 5E). Cells were grown in the  
660 presence of increasing concentrations of AZ1 for 72 hours, followed by *in vivo*  
661 exposure to propidium iodide (PI) as a marker for dead cells (Figure 5E) and  
662 immune- fluorescent staining of the proliferative marker Ki67 (Figure 5D). While the  
663 non-oncogenic BEAS-2B<sup>DIF</sup> showed weak reduction in cell proliferation and mild  
664 increase in nuclear PI positive cells, BEAS-2B<sup>ONC</sup> cells, irrespective of oncogenic  
665 driver, significantly reduced cell proliferation in an AZ1 concentration dependent  
666 fashion (Figure 5D). Additionally, when BEAS-2B<sup>ONC</sup> cells were exposed to AZ1  
667 concentrations reaching or exciding the oncogene corresponding IC<sub>50</sub>, PI  
668 incorporation was significantly enriched (Figure 5D and 5E). Surprisingly,  
669 BRAF<sup>V600E</sup> transformed BEAS-2B demonstrated a high degree of sensitivity  
670 towards AZ1 (Figure 5E), as it was previously reported that, in melanoma, loss of  
671 USP28 was required to induce oncogenic transformation and resistance.

672

673 Overall, our data demonstrated that USP28 is required to maintain tumour cell  
674 proliferation and survival *in cellulo*, hence, tumour cells become addicted to USP28.

675

676 ***Inhibition of USP28 via AZ1 ‘resets’ the proteome of oncogenic transduced***  
677 ***cells towards a ‘non-oncogenic’ state and induces pro-apoptotic signatures***

678

679 To gather further insights into how targeting of USP28 via AZ1 affects oncogenic  
680 transduced BEAS-2B cells, we conducted mass spectrometric analysis and  
681 compared the proteome of control and oncogenic transduced cells upon exposure to  
682 AZ1 (Figure S6A). Principal component analysis identified that oncogenic



683 transduction resulted in distinct changes of the proteome (Figure 6A and Figure  
684 S6B). Not only were the proteomes of BEAS-2B<sup>onc</sup> different when compared to non-  
685 oncogenic cells, but the oncogenic driver used established distinct proteomic  
686 patterns (Figure 6A). Upon exposure to AZ1, the proteomes of BEAS-2B<sup>onc</sup>,  
687 however, significantly changed and clustered with the expression of non-oncogenic  
688 BEAS-2B (Figure 6A and S6C). Analysing the proteome of the three BEAS-2B<sup>onc</sup> cell  
689 lines post AZ1 exposure revealed that a set of proteins dysregulated during  
690 oncogenic transformation was commonly affected in an AZ1 dependent fashion; 45  
691 proteins were decreased and 29 proteins commonly increased in BEAS-2B<sup>onc</sup>  
692 (Figure 6B, 6C and S6D). Proteins upregulated in EGFR858R transduced BEAS-2B  
693 were repressed upon exposure to AZ1, while proteins decreased during the course  
694 of oncogenic transformation enriched upon blockage of USP28 activity (Figure 6C,  
695 6D and S6D). Addition of 15  $\mu$ M AZ1 for 72 hours, however, not only reduced the  
696 abundance of proto-oncogenes, but re-shaped global protein abundance, closer  
697 resembling non-oncogenic BEAS-2B (Figure 6C and 6D). Inhibition of USP28 via  
698 AZ1 in oncogenic transduced BEAS-2B significantly repressed the abundance of  
699 proteins involved in negative regulation of the ubiquitin proteasome system,  
700 decreased RTK/growth factor signalling and vesicle transport, while oncogenic  
701 BEAS-2B upregulated proteins involved in differentiation, immune signalling,  
702 apoptosis and necrosis (Figure 6E).

703

704 Hence, acute inhibition of USP28 via AZ1 decreases the amount of proto-  
705 oncogenes, thereby affecting global protein abundance. USP28 is required to  
706 accommodate oncogenic transformation and to suppress anti-proliferative and pro-  
707 apoptotic signatures.

708

### 709 ***USP28 inhibition potentiates targeted molecular therapy***

710

711 To investigate if USP28 is a putative prognostic marker for NSCLC, we analysed  
712 public available datasets and observed that USP28 expression significantly  
713 correlates with progression free survival (PFS,  $p=4.6e-05$ ), Figure 7A and S7A). In  
714 the Post Progression Survival cohort, elevated expression of USP28 directly  
715 correlated with shortened survival (overall and Stage I, S7A and S7B). These data  
716 suggest that USP28 levels strongly determine the survival of the NSCLC patients in  
717 response to therapy.

718

719 Since NSCLC is a genetically very heterogeneous tumour type, next, we wondered if  
720 patient survival depended on the combination of oncogenic driver and the expression  
721 of USP28 (Figure 7B and S7C). Indeed, the analysis of public available data leads to  
722 the suggestion that, irrespective of oncogenic driver, an increased expression of  
723 USP28 significantly shortens survival for tumours driven by mutations in the  
724 oncogenes EGFR ( $\Delta 574$  days), PIK3CA ( $\Delta 177$  days) or BRAF ( $\Delta 922$  days), while in  
725 tumours driven by mutations in genes of the RAS family, USP28 had very little effect

726 on patient survival ( $\Delta$ 58 days, Figure 7B). These data suggest that USP28 is a  
727 suitable prognostic marker and oncogene in NSCLC.

728 As cancer panel sequencing is implemented in the clinics and pathway-specific  
729 inhibitors available, we were wondering if disruption of the oncogenic pathways  
730 would directly affect USP28 and hence, the abundance of its downstream effectors.  
731 Analysis of publicly available data regarding putative drug sensitivity of tumour cells  
732 in direct correlation to USP28 expression scored the PIK3-, EGFR- and MAPK  
733 pathway as top hits (Figure 7C), directly confirmed our experimental data regarding  
734 USP28 expression relative to oncogenic drivers. Since several potent pathway  
735 inhibitors are readily available (Figure 7D), we wondered if targeted therapy would  
736 synergize with targeted inhibition of USP28 via AZ1. To this end, we exposed our  
737 BEAS-2B<sup>ONC</sup> cell lines to either a selective inhibitor (EGFRL858R= Gefitinib;  
738 PIK3CAH1047R= Buparlisib; BRAFV600E= Vemurafenib), AZ1, or a combination  
739 thereof for 24 hours, followed by immunoblotting against USP28 and its substrates  
740 (Figure 7E). Selective pathway interference was evaluated by immunoblotting  
741 (Figure S7D). Monotherapy via selective pathway inhibitors affected downstream  
742 signalling cascades, reduced the abundance of USP28, led to a reduction in the  
743 protein levels of NOTCH1, c-MYC and c-JUN and reduced cell viability (Figure 7E  
744 and S7E). Similar effects were observed by administering AZ1; treated cells showed  
745 a reduction in USP28 abundance, along with reduced protein levels of its substrates  
746 and decreased viability (Figure 7E and S7E). Combinatorial treatment, however,  
747 significantly reduced the amount of USP28 and diminished the abundance of  
748 NOTCH1, cMYC and cJUN (Figure 7E). Not only does co-treatment with AZ1  
749 sensitize BEAS-2B<sup>ONC</sup> cells to targeted therapy, but it synergises with Gefitinib,  
750 Bupalislib and Vemurafenib, as seen by viability assays in BEAS-2B<sup>ONC</sup> cells (Figure  
751 7F). The synergistic effect of AZ1 and targeted therapy does not only stem from  
752 impairment of tumour cell proliferation, but also leads to onset of cell death, as seen  
753 by Ki67 expression and PI incorporation experiments of BEAS-2B<sup>ONC</sup> cells cultivated  
754 for 72 hours in the presence of the single compounds or combinations thereof at  
755 synergistic concentrations (AZ1: 7.5  $\mu$ M, Gefitinib: 7.5  $\mu$ M; Buparlisib: 0.5  $\mu$ M;  
756 Vemurafenib: 7.5  $\mu$ M; Figure 7G, H and S7E). Here, exposure to 7.5  $\mu$ M AZ1 did not  
757 affect proliferation nor induced cell death (Figure 7G and H). While monotherapy with  
758 targeted inhibitors led to a reduction in proliferation, it did not result in cell death, as  
759 seen by loss of Ki67 expression and the absence of PI incorporation (Figure 7G and  
760 H). The combinatorial treatment, however, resulted in a significant increase in PI  
761 positive cells, while maintaining a proliferative block.

762  
763 USP28 therefore, functions as a signal amplifier downstream of various oncogenic  
764 signalling cascades and is required to allow oncogenic transformation. Its inhibition  
765 potentiates targeted therapy by impairing the protein stability of oncogenic  
766 transcription factors, required to maintain tumour cell proliferation, and presents a  
767 promising target for drug development.

768

769 **Discussion**

770

771 Oncogenic transformation of somatic cells is a multistage process frequently starting  
772 with the inactivation of tumor suppressors and subsequent gain of activating  
773 mutations in oncogenic drivers, such as members of the PI3K or MAPK family.  
774 These changes result in the increased abundance of proto-oncogenes, such as c-  
775 MYC<sup>(33)</sup>, JUN<sup>(34)</sup> or NOTCH, driving cell proliferation, dedifferentiation, metabolic  
776 changes, DNA damage control, immune evasion and proteostatic stress  
777 management, the 'hallmarks of cancer'(23).

778

779 Cells undergoing transformation partially counter this intrinsic stress by re-adjusting  
780 the UPS. USP28 is involved in the control of a plethora of biological processes. It is  
781 involved in the regulation of cell proliferation and differentiation via its ability to  
782 regulate the abundance of the proto-oncogenes, such as c-MYC, c-JUN or NOTCH  
783 (Figure 8A) (29). It is involved in transcriptional control via regulating the abundance  
784 of the histone modifier LSD1/KDM1A(35) and it is part of the DNA damage  
785 machinery, where it interacts with ATM(36), CLSPN(37), or TP53BP1(38).

786

787 Overall, USP28 functions as a proto-oncogene and contributes to establishing the  
788 hallmarks of cancer in cells undergoing oncogenic transformation, at least in  
789 lung(22). Here, USP28 is expressed in the stem cell niche and elevated abundance  
790 detected in 'cells of origin'. Its upregulation is an early event, as already low grade  
791 tumours showed enhanced abundance for this particular DUB, and its expression  
792 coincided with shortened overall survival. In a cellular multi-stage transformation  
793 model, we were able to recapitulate the stepwise increase in USP28 abundance and  
794 enhanced activity, which occurred independent to the oncogenic driver present.  
795 USP28 is a transcriptional target of its own substrates(29), and via a feed forward  
796 loop, increased in cancer compared to normal. Irrespective of oncogenic driver,  
797 interference with USP28 abundance or activity suppressed tumour cell growth and  
798 survival of transformed lung cells *in vitro* and *in vivo*. Inhibition of USP28 via the  
799 small molecule inhibitor AZ1 restored the proteome of oncogenic transformed BEAS-  
800 2B cells towards a pre-malignant state, demonstrating that interference with USP28  
801 abundance and activity has a far-reaching biological impact. USP28 is a downstream  
802 target of RTK signaling cascades and required to establish oncogenic transformation  
803 by its ability to control the abundance of proto-oncogenes. The inhibition of the DUB  
804 not only repressed tumour cell growth but led to a pro-apoptotic phenotype,  
805 predominantly in oncogenic transformed cells, while control cells were not affected.  
806 Here, the cell cycle was affected, leading to a reduction in proliferation.

807

808 This is in stark contrast to two recent reports. In a small cohort of melanoma  
809 patients, where tumours are predominantly driven by mutant BRAF(V600E), USP28  
810 is genetically lost(39). These USP28 mutant patients present enhanced MAPK  
811 signaling via hyperstabilisation of RAF family members and resistance to BRAF  
812 inhibitors. Here, loss of USP28 presents a negative survival marker. The second  
813 study identified that, in melanoma cells, USP28 is cleaved by caspase 8 to overcome

814 G2/M cell cycle arrest in a TP53 dependent fashion(40). Loss of USP28 in tumour  
815 cells is favored as it results in TP53 protein destabilization, thereby establishing a  
816 switch of cell fate, from apoptosis towards mitosis. Hence, USP28 functions as a  
817 tumour suppressor in melanoma(41). In line with these reports, we could not detect a  
818 correlation between USP28 and BRAF expression in human skin cancer samples.  
819 This could be indicating that this tumour entity indeed does not rely on the DUB and  
820 hence, alternative mechanisms deviating from our observation in lung and SCC, are  
821 possible.

822

823 In lung, and as previously reported for squamous cell carcinoma(22), targeting  
824 USP28 presents a suitable lever for therapeutic engagement, as one could propose  
825 that at least in lung, tumour cells become addicted to USP28. In line with this  
826 hypothesis, we indeed did observe that loss of USP28 reduced oncogenic cell  
827 proliferation and its genetic loss impaired tumour onset *in vivo*. The inhibition of  
828 USP28, via a small molecule inhibitor AZ1, induced pro-apoptotic signaling in cells  
829 expressing potent oncogenic driver mutants. In lung, the expression of USP28  
830 directly correlated with shortened patient survival, irrespective of oncogenic driver.  
831 As USP28 functions as an 'amplifier' downstream of RTKs, its inhibition cooperated  
832 with personalized targeted therapy against specific oncogenic driver mutations  
833 (Figure 8B).

834

835 Overall, our data suggest that targeting USP28 protein abundance and activity  
836 already at an early stage, therefore, is a promising strategy for the treatment of lung  
837 tumours in combination to personalized targeted therapy.

838

### 839 **Acknowledgements**

840 We are grateful to the animal facility and Barbara Bauer at the Biocenter, University  
841 Würzburg. C.P.G. and O.H. are supported by the German Cancer Aid via grant  
842 70112491, M.R. is funded by the DFG-GRK 2243 and IZKF B335. M.E.D. and M.R.  
843 are funded by the German Israeli Foundation grant 1431. T. F. is funded by the IZKF  
844 program Z2/CS-1.

845

### 846 **Conflict of Interest:**

847 The authors declare no potential conflicts of interest.

848

849

850

851

852

853

854

855

856

857

858

859

860

861

862

863

864

865

866

867

868

869

870

871

872

873

## 874 **References**

875

876 1. Alexander M, Kim SY, and Cheng H. Update 2020: Management of Non-Small Cell  
877 Lung Cancer. *Lung*. 2020;198(6):897-907.

878 2. Shin JY, Yoon JK, and Marwaha G. Progress in the Treatment and Outcomes for Early-  
879 Stage Non-Small Cell Lung Cancer. *Lung*. 2018;196(3):351-8.

880 3. Hopstaken JS, de Ruiter JC, Damhuis RAM, de Langen AJ, van Diessen JNA, Klomp  
881 HM, et al. Stage I non-small cell lung cancer: Treatment modalities, Dutch daily  
882 practice and future perspectives. *Cancer Treat Res Commun*. 2021;28:100404.

883 4. McDonald F, De Waele M, Hendriks LE, Faivre-Finn C, Dingemans AC, and Van Schil  
884 PE. Management of stage I and II nonsmall cell lung cancer. *Eur Respir J*. 2017;49(1).

885 5. Stokes WA, Bronsert MR, Meguid RA, Blum MG, Jones BL, Koshy M, et al. Post-  
886 Treatment Mortality After Surgery and Stereotactic Body Radiotherapy for Early-  
887 Stage Non-Small-Cell Lung Cancer. *J Clin Oncol*. 2018;36(7):642-51.

888 6. Wang F, Wang S, and Zhou Q. The Resistance Mechanisms of Lung Cancer  
889 Immunotherapy. *Front Oncol*. 2020;10:568059.

890 7. Aveic S, and Tonini GP. Resistance to receptor tyrosine kinase inhibitors in solid  
891 tumors: can we improve the cancer fighting strategy by blocking autophagy? *Cancer*  
892 *Cell Int*. 2016;16:62.

893 8. Park J, Cho J, and Song EJ. Ubiquitin-proteasome system (UPS) as a target for  
894 anticancer treatment. *Arch Pharm Res*. 2020;43(11):1144-61.

895 9. Almond JB, and Cohen GM. The proteasome: a novel target for cancer  
896 chemotherapy. *Leukemia*. 2002;16(4):433-43.

897 10. Fan Q, Wang Q, Cai R, Yuan H, and Xu M. The ubiquitin system: orchestrating cellular  
898 signals in non-small-cell lung cancer. *Cell Mol Biol Lett*. 2020;25:1.

- 899 11. Tsvetkov P, Adler J, Myers N, Biran A, Reuven N, and Shaul Y. Oncogenic addiction to  
900 high 26S proteasome level. *Cell Death Dis.* 2018;9(7):773.
- 901 12. Fhu CW, and Ali A. Dysregulation of the Ubiquitin Proteasome System in Human  
902 Malignancies: A Window for Therapeutic Intervention. *Cancers (Basel).* 2021;13(7).
- 903 13. Schauer NJ, Magin RS, Liu X, Doherty LM, and Buhrlage SJ. Advances in Discovering  
904 Deubiquitinating Enzyme (DUB) Inhibitors. *J Med Chem.* 2020;63(6):2731-50.
- 905 14. D'Arcy P, Wang X, and Linder S. Deubiquitinase inhibition as a cancer therapeutic  
906 strategy. *Pharmacol Ther.* 2015;147:32-54.
- 907 15. Antao AM, Tyagi A, Kim KS, and Ramakrishna S. Advances in Deubiquitinating  
908 Enzyme Inhibition and Applications in Cancer Therapeutics. *Cancers (Basel).*  
909 2020;12(6).
- 910 16. Wrigley JD, Gavory G, Simpson I, Preston M, Plant H, Bradley J, et al. Identification  
911 and Characterization of Dual Inhibitors of the USP25/28 Deubiquitinating Enzyme  
912 Subfamily. *ACS Chem Biol.* 2017;12(12):3113-25.
- 913 17. Prieto-Garcia C, Hartmann O, Reissland M, Braun F, Fischer T, Walz S, et al.  
914 Maintaining protein stability of Np63 via USP28 is required by squamous cancer cells.  
915 *EMBO Mol Med.* 2020:e11101.
- 916 18. Kim CF, Jackson EL, Woolfenden AE, Lawrence S, Babar I, Vogel S, et al. Identification  
917 of bronchioalveolar stem cells in normal lung and lung cancer. *Cell.* 2005;121(6):823-  
918 35.
- 919 19. Ferone G, Lee MC, Sage J, and Berns A. Cells of origin of lung cancers: lessons from  
920 mouse studies. *Genes Dev.* 2020;34(15-16):1017-32.
- 921 20. Sanchez-Danes A, and Blanpain C. Deciphering the cells of origin of squamous cell  
922 carcinomas. *Nat Rev Cancer.* 2018;18(9):549-61.
- 923 21. Ferone G, Song JY, Sutherland KD, Bhaskaran R, Monkhorst K, Lambooi JP, et al.  
924 SOX2 Is the Determining Oncogenic Switch in Promoting Lung Squamous Cell  
925 Carcinoma from Different Cells of Origin. *Cancer Cell.* 2016;30(4):519-32.
- 926 22. Prieto-Garcia C, Hartmann O, Reissland M, Braun F, Fischer T, Walz S, et al.  
927 Maintaining protein stability of Np63 via USP28 is required by squamous cancer cells.  
928 *EMBO Mol Med.* 2020;12(4):e11101.
- 929 23. Hartmann O, Reissland M, Maier CR, Fischer T, Prieto-Garcia C, Baluapuri A, et al.  
930 Implementation of CRISPR/Cas9 Genome Editing to Generate Murine Lung Cancer  
931 Models That Depict the Mutational Landscape of Human Disease. *Front Cell Dev Biol.*  
932 2021;9:641618.
- 933 24. Platt RJ, Chen S, Zhou Y, Yim MJ, Swiech L, Kempton HR, et al. CRISPR-Cas9 knockin  
934 mice for genome editing and cancer modeling. *Cell.* 2014;159(2):440-55.
- 935 25. Zhao F, and Klimecki WT. Culture conditions profoundly impact phenotype in BEAS-  
936 2B, a human pulmonary epithelial model. *J Appl Toxicol.* 2015;35(8):945-51.
- 937 26. Sakamoto O, Iwama A, Amitani R, Takehara T, Yamaguchi N, Yamamoto T, et al. Role  
938 of macrophage-stimulating protein and its receptor, RON tyrosine kinase, in ciliary  
939 motility. *J Clin Invest.* 1997;99(4):701-9.



- 940 27. Temko D, Tomlinson IPM, Severini S, Schuster-Bockler B, and Graham TA. The effects  
941 of mutational processes and selection on driver mutations across cancer types. *Nat*  
942 *Commun.* 2018;9(1):1857.
- 943 28. Arason AJ, Jonsdottir HR, Halldorsson S, Benediktsdottir BE, Bergthorsson JT,  
944 Ingthorsson S, et al. deltaNp63 has a role in maintaining epithelial integrity in airway  
945 epithelium. *PLoS One.* 2014;9(2):e88683.
- 946 29. Diefenbacher ME, Popov N, Blake SM, Schulein-Volk C, Nye E, Spencer-Dene B, et al.  
947 The deubiquitinase USP28 controls intestinal homeostasis and promotes colorectal  
948 cancer. *J Clin Invest.* 2014;124(8):3407-18.
- 949 30. Serra RW, Fang M, Park SM, Hutchinson L, and Green MR. A KRAS-directed  
950 transcriptional silencing pathway that mediates the CpG island methylator  
951 phenotype. *Elife.* 2014;3:e02313.
- 952 31. Bonamy C, Sechet E, Amiot A, Alam A, Mourez M, Fraisse L, et al. Expression of the  
953 human antimicrobial peptide beta-defensin-1 is repressed by the EGFR-ERK-MYC axis  
954 in colonic epithelial cells. *Sci Rep.* 2018;8(1):18043.
- 955 32. Kim H, Park SY, Jung J, Kim JH, Hahn SY, Shin JH, et al. Improved survival after early  
956 detection of asymptomatic distant metastasis in patients with thyroid cancer. *Sci*  
957 *Rep.* 2019;9(1):18745.
- 958 33. Seo AN, Yang JM, Kim H, Jheon S, Kim K, Lee CT, et al. Clinicopathologic and  
959 prognostic significance of c-MYC copy number gain in lung adenocarcinomas. *Br J*  
960 *Cancer.* 2014;110(11):2688-99.
- 961 34. Ruiz EJ, Lan L, Diefenbacher ME, Riising EM, Da Costa C, Chakraborty A, et al. JunD,  
962 not c-Jun, is the AP-1 transcription factor required for Ras-induced lung cancer. *JCI*  
963 *Insight.* 2021;6(13).
- 964 35. Wu Y, Wang Y, Yang XH, Kang T, Zhao Y, Wang C, et al. The deubiquitinase USP28  
965 stabilizes LSD1 and confers stem-cell-like traits to breast cancer cells. *Cell Rep.*  
966 2013;5(1):224-36.
- 967 36. Zhang D, Zaugg K, Mak TW, and Elledge SJ. A role for the deubiquitinating enzyme  
968 USP28 in control of the DNA-damage response. *Cell.* 2006;126(3):529-42.
- 969 37. Ito F, Yoshimoto C, Yamada Y, Sudo T, and Kobayashi H. The HNF-1beta-USP28-  
970 Claspin pathway upregulates DNA damage-induced Chk1 activation in ovarian clear  
971 cell carcinoma. *Oncotarget.* 2018;9(25):17512-22.
- 972 38. Knobel PA, Belotserkovskaya R, Galanty Y, Schmidt CK, Jackson SP, and Stracker TH.  
973 USP28 is recruited to sites of DNA damage by the tandem BRCT domains of 53BP1  
974 but plays a minor role in double-strand break metabolism. *Mol Cell Biol.*  
975 2014;34(11):2062-74.
- 976 39. Saei A, Palafox M, Benoukraf T, Kumari N, Jaynes PW, Iyengar PV, et al. Loss of  
977 USP28-mediated BRAF degradation drives resistance to RAF cancer therapies. *J Exp*  
978 *Med.* 2018;215(7):1913-28.

- 979 40. Muller I, Strozyk E, Schindler S, Beissert S, Oo HZ, Sauter T, et al. Cancer Cells Employ  
980 Nuclear Caspase-8 to Overcome the p53-Dependent G2/M Checkpoint through  
981 Cleavage of USP28. *Mol Cell*. 2020;77(5):970-84 e7.
- 982 41. Soysouvanh F, Giuliano S, Habel N, El-Hachem N, Pisibon C, Bertolotto C, et al. An  
983 Update on the Role of Ubiquitination in Melanoma Development and Therapies. *J*  
984 *Clin Med*. 2021;10(5).

985  
986  
987  
988  
989  
990  
991  
992  
993  
994  
995  
996

#### 997 **Figure Legends**

998  
999  
1000

#### 999 **Figure 1: *USP28* is expressed in human ‘cell-of-origin’ for NSCLC and** 1000 ***upregulated irrespective of lung tumour subtype***

- 1001 A) Schematic representation of the cellular composition of the tracheal, bronchio-  
1002 alveolar and alveolar compartment. Highlighted are the respective tissue  
1003 residing stem cells. Trachea = basal cells, Bronchio-alveolar duct junction =  
1004 BADJ cells, Alveolar compartment = AT2 cells.
- 1005 B) Immuno-histochemical staining of endogenous USP28 in patient lung  
1006 resected material. Shown are representative images of alveolar, bronchial and  
1007 tracheal sections.
- 1008 C) Expression of USP28 in non-transformed and NSCLC Adenocarcinoma  
1009 (ADC) and Squamous Cell Carcinoma (SCC) samples, relative to tumour  
1010 stage (T1-T4). Public available data. p-values were calculated using two-tailed  
1011 T-test statistical analysis. Plot was generated using the online tool  
1012 [www.gepia2.cancer-pku.cn](http://www.gepia2.cancer-pku.cn).
- 1013 D) Immuno-histochemical staining of USP28 on human NSCLC tissue micro  
1014 arrays of ADC and SCC origin, ranging from Grade 1 to 3. Where applicable,  
1015 non-transformed adjacent tissue was included. Shown are representative  
1016 images per tumour type.
- 1017 E) Immuno-histochemical staining of USP28 on human lung cancer tissue micro  
1018 arrays of various lung cancer subtypes. Where applicable, non-transformed  
1019 adjacent tissue was included. lung resected material. Shown are  
1020 representative images per tumour type.

- 1021 F) Kaplan-Meier plots of NSCLC patient Overall Survival (OS), relative to USP28  
1022 expression, at Stage 1 ( $p < 0.0005$ ), Stage 2 ( $p = 0.02$ ) to Stage 3 ( $p = 0.55$ ).  
1023 Data was generated using the online tool [www.kmplot.com](http://www.kmplot.com).  
1024 G) Kaplan-Meier plots of NSCLC ADC and SCC patient Overall Survival (OS),  
1025 relative to USP28 expression, at Stage 1 (ADC  $p = 0.0063$ ; SCC  $p = 0.00057$ ).  
1026 Data was generated using the online tool [www.kmplot.com](http://www.kmplot.com).

1027

1028 See also Supplementary Figure S1.

1029

1030 Figure 2: ***USP28 is expressed in murine lung stem cells and required to***  
1031 ***establish oncogenic transformation in vivo.***

- 1032 A) Immuno-histochemical staining of endogenous Usp28 in murine lung wild type  
1033 tissue. Shown are representative images of alveolar, bronchial, bronchio-  
1034 alveolar duct junction and tracheal sections. Red boxes indicate highlighted  
1035 areas.  
1036 B) *Ex vivo* onset of oncogenic transduction by CRISPR mediated gene editing  
1037 and deletion of *Trp53* and mutation of *KRas* to *KRas<sup>G12D</sup>* (KP) upon AAV  
1038 infection of organotypic lung slice cultures. Lung slice cultures were generated  
1039 from *C57Bl6/J-Rosa26<sup>Sor-CAGG-Cas9-IRES-eGFP</sup>* mice and AAV encodes mCherry  
1040 as marker. Fluorescent images of lung slice cultures post infection with AAV.  
1041 GFP = lung; RFP = AAV infected lung epithelial cells. Tissue sections were  
1042 harvested and subjected to RNA isolation, followed by RT-PCR analysis of  
1043 *Usp28* mRNA expression in control and KP infected slices.  $n = 3$  sections  
1044 each.  $p$ -values were calculated using two-tailed T-test statistical analysis.  
1045 C) Schematic representation of *in vivo* CRISPR gene editing to delete *Trp53* and  
1046 mutate *KRas* to *KRas<sup>G12D</sup>* (KP) upon intratracheal administering of AAV.  
1047 Animals are sacrificed 12 weeks post infection.  
1048 D) Representative images of immuno-histochemical staining against endogenous  
1049 Usp28, Nkx2-1/Ttf-1, c-Jun, Notch1 and c-Myc in murine lungs infected with  
1050 either control virus (WT) or KP. Shown are representative tumours spanning  
1051 grade 1 to 3, with a low and high magnification of individual tumour areas.  $n = 3$   
1052 E) Schematic representation of *in vivo* CRISPR gene editing to delete *Trp53*,  
1053 mutate *KRas* to *KRas<sup>G12D</sup>* (KP) or co-delete *Usp28* (KPU) upon intratracheal  
1054 administering of AAV. Animals are sacrificed 4 weeks post infection.  $n = 6$ .  
1055 F) Representative H&E images KP and KPU 4 weeks post infection.  
1056 Quantification of tumour burden per animal.  $n = 6$ .  $p$ -values were calculated  
1057 using two-tailed T-test statistical analysis.

1058

1059 See also Supplementary Figure S2.

1060

1061 Figure 3: ***USP28 is increased during early transformation in human BEAS-2B***  
1062 ***differentiation assay***

- 1063 A) Schematic model of the trans-differentiation by culturing stem cell like,  
1064 undifferentiated BEAS-2B (BEAS-2B<sup>UND</sup>) in the presence of 10% fetal calf  
1065 serum to induce squamous like differentiation, BEAS-2B<sup>DIF</sup>.  
1066 B) Representative brightfield-images of BEAS-2B prior and post serum induced  
1067 trans-differentiation (72 hours in the presence of 10% FCS, UND to DIF).  
1068 Immunoblot against endogenous USP28 and  $\Delta$ NP63 of BEAS-2B<sup>UND</sup> and  
1069 BEAS-2B<sup>DIF</sup>. ACTIN served as loading control. Representative blot of n=3.  
1070 C) Immunofluorescence of endogenous USP28 prior and post differentiation.  
1071 USP28 in green, ACTIN in red, DAPI as nuclear counterstain.  
1072 D) Immunoblot against endogenous USP28 in the absence or presence of a  
1073 Ubiquitin suicide probe (warhead, WH) to assess USP28 enzymatic activity in  
1074 undifferentiated and differentiated BEAS-2B cells. Upon binding to the activity  
1075 probe, a shift in molecular weight is observed, indicative of enzymatic activity  
1076 (see arrows). ACTIN served as loading control. Representative immunoblot of  
1077 n=3.  
1078 E) Representative brightfield-images of BEAS-2B prior and post culture in serum  
1079 induced trans-differentiation conditions, in the presence or absence of the  
1080 USP28 inhibitor AZ1 (15 $\mu$ M, 72 hours). Immunoblot against endogenous  
1081 USP28 and  $\Delta$ NP63 of BEAS-2B<sup>UND</sup> exposed to either 10% FCS or 10% FCS  
1082 and 15 $\mu$ M AZ1. ACTIN served as loading control. Representative blot of n=3.  
1083

1084 Figure 4: ***Oncogenic transformation of BEAS-2B<sup>DIF</sup> via EGFR-PI3K-MAPK***  
1085 ***pathway upregulate USP28 and accelerates tumour cell growth***

- 1086 A) Frequently occurring genetic alteration in recurring oncogenic drivers found in  
1087 NSCLC (ADC and SCC). Oncoprints generated with the online tool  
1088 [www.cbioportal.org](http://www.cbioportal.org).  
1089 B) mRNA expression Spearman's correlation between USP28 and EGFR,  
1090 HRAS, BRAF or PIK3CA in NSCLC (SCC and ADC). Correlation and p-value  
1091 generated with the online tool GEPIA [www.gepia2.cancer-pku.cn/](http://www.gepia2.cancer-pku.cn/).  
1092 C) Immunoblot against endogenous USP28 and the oncogenic transcription  
1093 factor  $\Delta$ NP63 either BEAS-2B<sup>DIF</sup> or BEAS-2B<sup>DIF</sup> upon retroviral transduction to  
1094 express the indicated oncogenes EGFR (wild type (WT) and L858R), HRAS  
1095 (G12D), BRAF (V600E) and PIK3CA (wild type (WT), E545K and H1047R),  
1096 respectively. ACTIN served as loading control. Representative immunoblot of  
1097 n=3.  
1098 D) RT-PCR of USP28, the SCC transcription factor  $\Delta$ NP63 and its target  
1099 Cytokeratin 14 (KRT14) in BEAS-2B<sup>UND</sup>, BEAS-2B<sup>DIF</sup> or the various BEAS-  
1100 2B<sup>ONC</sup> as presented in C). Shown are Log2fold change expression data,  
1101 relative to ACTIN and normalized to the respective expression in BEAS-2B<sup>UND</sup>  
1102 and standard deviation. Shown are mean values and standard deviation of  
1103 n=3  
1104 E) Relative cell numbers and assessment of growth capacity of BEAS-2B<sup>UND</sup>,  
1105 BEAS-2B<sup>DIF</sup> or the various BEAS-2B<sup>ONC</sup> over a total of 4 days. Cell numbers  
1106 were analyzed every day. Shown are mean values and standard deviation.

1107 n=3 experiments. p-values were calculated using two-tailed T-test statistical  
1108 analysis.

1109 F) Schematic model of the various stages of oncogenic transformation, as  
1110 recapitulated by the trans-differentiation from BEAS-2B<sup>UND</sup> to BEAS-2B<sup>DIF</sup>,  
1111 and from BEAS-2B<sup>DIF</sup> to BEAS-2B<sup>ONC</sup> (oncogenic transformed BEAS-2B<sup>DIF</sup>).  
1112 The observed increases recapitulate the increase in USP28 protein  
1113 abundance as seen in human NSCLC samples.

1114

1115 See also Supplementary Figure S3 and S4.

1116

1117 Figure 5: ***Malignant transformation renders tumour cells dependent on USP28***

1118 A) Immunoblot showing protein abundance of USP28 in BEAS-2B<sup>DIF</sup> upon  
1119 lentiviral transduction with either a control or a doxycycline inducible  
1120 overexpression of murine Usp28. BEAS-2B<sup>DIF</sup> control and mUsp28 cells were  
1121 cultured in the presence of 1µg/ml doxycycline for 72 hours prior to  
1122 immunoblotting. ACTIN served as loading control. For growth analysis, cells  
1123 were pre-cultured for 72 hours in the presence of 1µg/ml doxycycline,  
1124 followed by re-seeding and counting of cells at day 1, day 3 and day 6. Shown  
1125 are mean values and standard deviation of n=3. p-values were calculated  
1126 using two-tailed T-test statistical analysis.

1127 B) Immunoblot showing protein abundance of USP28 in oncogenic transduced  
1128 BEAS-2B<sup>ONC</sup> (EGFRL858R, PIK3CA L1047R and BRAFV600E) upon  
1129 lentiviral transduction with either a control or two individual constitutive shRNA  
1130 targeting USP28. ACTIN served as loading control. For growth analysis, cells  
1131 were seeded at equal cell density and counted at day 1, day 2 and day 4.  
1132 Shown are mean values and standard deviation of n=3.

1133 C) Immunoblots against endogenous USP28 and its substrates NOTCH1, c-MYC  
1134 and c-JUN in either BEAS-2B<sup>DIF</sup> or oncogenic transduced BEAS-2B<sup>ONC</sup>  
1135 (EGFRL858R, PIK3CA L1047R and BRAFV600E) upon exposure to either  
1136 DMSO or 15µM AZ1 for 24 hours. VINCULIN served as loading control.

1137 D) Immunofluorescence of Ki-67 expression in BEAS-2B<sup>DIF</sup> or oncogenic  
1138 transduced BEAS-2B<sup>ONC</sup> (EGFRL858R, PIK3CA L1047R and BRAFV600E)  
1139 cultured in the presence of increasing concentrations of AZ1 (0 (DMSO),  
1140 7.5µM, 15 µM, 30 µM) for 72 hours to assess effects in cell proliferation.  
1141 Shown are representative cells. Quantification of Ki-67 expression in 30-45  
1142 20x fields from independent wells per condition. DAPI served as nuclear  
1143 marker. Shown are mean values and standard deviation. p-values were  
1144 calculated using two-tailed T-test statistical analysis.

1145 E) Immunofluorescence of propidium iodide (PI) incorporation in BEAS-2B<sup>DIF</sup> or  
1146 oncogenic transduced BEAS-2B<sup>ONC</sup> (EGFRL858R, PIK3CA L1047R and  
1147 BRAFV600E) cultured in the presence of increasing concentrations of AZ1 (0  
1148 (DMSO), 7.5µM, 15 µM, 30 µM) for 72 hours to assess effects on cell survival  
1149 and apoptosis. Shown are representative cells. Quantification of PI positive

1150 cells in 30-45 20x fields from independent wells per condition. DAPI served as  
1151 nuclear marker. Shown are mean values and standard deviation. p-values  
1152 were calculated using two-tailed T-test statistical analysis.

1153

1154 See also Supplementary Figure S5.

1155

1156 Figure 6: ***Inhibition of USP28 via AZ1 ‘resets’ the proteome of oncogenic***  
1157 ***transduced cells towards a ‘non-oncogenic’ state and induces pro-apoptotic***  
1158 ***signatures***

1159 A) Principal Component Analysis (PCA) of the whole proteome of BEAS-2B<sup>DIF</sup>  
1160 and BEAS-2B<sup>ONC</sup> (EGFRL858R, PIK3CA L1047R), treated with either 15  $\mu$ M  
1161 AZ1 for 72 hours or exposed to control solvent (DMSO). N=3 samples.  
1162 Analysis generated with Clustvis online tool (<https://biit.cs.ut.ee/clustvis>).

1163 B) Venn diagram illustrating proteins changed upon exposure of BEAS-2B<sup>ONC</sup>  
1164 (EGFRL858R, PIK3CA L1047R) to 15  $\mu$ M AZ1 for 72 hours. Highlighted are  
1165 numbers of proteins dysregulated during oncogenic transformation (BEAS-2B  
1166  $\rightarrow$  BEAS-2B<sup>ONC</sup>) and decreased or increased upon AZ1 exposure. Discreet or  
1167 common deregulated protein numbers are indicated within the corresponding  
1168 overlapping graphs. Common, oncogenic driver independent number of  
1169 deregulated proteins are highlighted in the center. Analysis of n=3 samples  
1170 per oncogenic driver.

1171 C) Heatmap of proteins identified in B) for BEAS-2B<sup>DIF</sup>, BEAS-2B<sup>EGFRL858R</sup> and  
1172 BEAS-2B<sup>EGFRL858R</sup> treated with 15  $\mu$ M AZ1 for 72 hours. Shown are n=3  
1173 experiments and data presented as Z score values. Red= high Z-score  
1174 protein abundance, blue = low Z-score protein abundance.

1175 D) Violin plots illustrating changes of BEAS-2B<sup>DIF</sup> and BEAS-2B<sup>ONC</sup> pre- and  
1176 post-treatment with 15  $\mu$ M AZ1 for 72 hours for decreased or increased  
1177 proteins identified in B). p-values were calculated using two-tailed T-test  
1178 statistical analysis. For Violin plot, white circles show the medians; box limits  
1179 indicate the 25th and 75th percentiles as determined by R software; whiskers  
1180 extend 1.5 times the interquartile range from the 25th and 75th percentiles;  
1181 polygons represent density estimates of data and extend to extreme values.  
1182 Violin plot were generated with BoxplotR. <http://shiny.chemgrid.org/boxplotr/>

1183 E) GO biological process significantly reduced or increased in BEAS-2B<sup>ONC</sup> upon  
1184 15  $\mu$ M AZ1 for 72 hours. The analysis was performed with the proteins  
1185 identified in B). The analysis was performed using the online tool Panther.  
1186 <http://www.pantherdb.org>

1187

1188 See also Supplementary Figure S6.

1189

1190 Figure 7: ***USP28 inhibition potentiates targeted molecular therapy***

1191



- 1192 A) Kaplan Meier plot of Progression free survival (PFS) of NSCLC patients  
1193 relative to USP28 mRNA expression. n=596 samples, p=<0.0005. Data  
1194 generated with the online tool [www.kmplot.com](http://www.kmplot.com).
- 1195 B) Analysis of public available datasets analysing USP28 mRNA expression and  
1196 Overall Survival (OS) in patients with mutations in the oncogenic driver  
1197 EGFR, RAS, PIK3CA or BRAF. Samples were divided in two groups based on  
1198 USP28 mRNA expression: High USP28 (higher than the median USP28  
1199 expression) and Low USP28 (lower than the median USP28 expression).  
1200 Survival days was determined for both groups. Data was obtained from the  
1201 online tool <https://xena.ucsc.edu/>. In box plots, the centre line reflects the  
1202 median and the upper and lower box limits indicate the first and third quartiles.  
1203 Whiskers extend 1.5x the IQR.
- 1204 C) Pearson correlation between sensitivity of EGFR-PI3K-MAPK inhibitors and  
1205 USP28 expression in human NSCLC cell lines. Data was generated with the  
1206 online tool Cancer Therapeutics Response Portal V2  
1207 (<https://portals.broadinstitute.org/ctrp/>). In plots, the lower line reflects the  
1208 median and the upper box limit indicates the first quartile. Whiskers extend  
1209 1.5x the IQR.
- 1210 D) Schematic representation of EGFR-PI3K-MAPK pathway analysed in this  
1211 study and potential pathway interference opportunities by EGFR-PI3K-MAPK  
1212 and AZ1 inhibitors. Green = EGFR-PI3K-MAPK inhibitors. Violet = AZ1.
- 1213 E) Immunoblots of BEAS-2B<sup>ONC</sup> (EGFRL858R, PIK3CA L1047R and  
1214 BRAFV600E) cultured in the presence of either control solvent (DMSO),  
1215 pathway specific inhibitors (EGFR: 20 µM Gefitinib; PIK3CA: 1µM Buparsilib;  
1216 BRAF: 20 µM Vemurafenib), 15 µM AZ1 or a combination thereof for 24  
1217 hours.
- 1218 F) BLISS synergism score of BEAS-2B<sup>ONC</sup> (EGFRL858R, PIK3CA L1047R and  
1219 BRAFV600E) cultured in the presence of either control solvent (DMSO),  
1220 pathway specific inhibitors (EGFR: Gefitinib; PIK3CA: Buparsilib; BRAF:  
1221 Vemurafenib), AZ1 and combination thereof for 72 hours at indicated  
1222 concentrations. Shown are representative DAPI images of cells 72 hours post  
1223 culture in the presence of DMSO, single treatment with 7.5 µM AZ1, 7.5 µM  
1224 Gefitinib, 0.5µM Buparlisib, 7.5µM Vemurafenib or combination of AZ1 with  
1225 the respective personalized molecular therapy for 72 hours. Synergism was  
1226 calculated by cell quantification of 30-45 20x fields from independent wells in  
1227 control (DMSO) and the indicated treated conditions.
- 1228 G) Immunofluorescence of Ki-67 expression in oncogenic transduced BEAS-  
1229 2B<sup>ONC</sup> (EGFRL858R, PIK3CA L1047R and BRAFV600E), cultured in the  
1230 presence of DMSO, single treatment with 7.5 µM AZ1, 7.5 µM Gefitinib,  
1231 0.5µM Buparlisib, 7.5µM Vemurafenib or combination of AZ1 with the  
1232 respective pathway inhibitor for 72 hours, to assess effects in cell proliferation.  
1233 Shown are representative cells. Quantification of Ki-67 expression in 30 to 45  
1234 20x fields from different wells in control (DMSO) and treated conditions. DAPI

1235 served as nuclear marker. Shown are mean values and standard deviation.  
1236 p-values were calculated using two-tailed T-test statistical analysis.

1237 H) Immunofluorescence of propidium iodide (PI) in vivo incorporation of  
1238 oncogenic transduced BEAS-2B<sup>ONC</sup> (EGFRL858R, PIK3CA L1047R and  
1239 BRAFV600E), cultured in the presence of DMSO, single treatment with 7.5  
1240  $\mu$ M AZ1, 7.5  $\mu$ M Gefitinib, 0.5 $\mu$ M Buparlisib, 7.5 $\mu$ M Vemurafenib or  
1241 combination of AZ1 with the respective pathway inhibitor for 72 hours, to  
1242 assess effects in cell proliferation. Shown are representative cells.  
1243 Quantification of PI positive cells in 30 to 45 20x fields from different wells in  
1244 control (DMSO) and treated conditions. DAPI served as nuclear marker.  
1245 Shown are mean values and standard deviation. p-values were calculated  
1246 using two-tailed T-test statistical analysis.

1247

1248 See also Supplementary Figure S7.

1249

1250 **Figure 8: USP28 enables oncogenic reprogramming of respiratory cells during**  
1251 **early transformation and its inhibition potentiates targeted molecular therapy.**

1252

1253 A) Schematic representation of the mechanism presented in this manuscript.  
1254 Oncogenic transformation via EGFR-PI3K-MAPK pathway increases USP28  
1255 transcription via c-MYC/ c-JUN. USP28 stabilizes the oncoproteins c-MYC/ c-  
1256 JUN establishing a direct feedback loop.

1257 B) Schematic representation of the synergy between EGFR-PI3K-MAPK  
1258 targeted molecular therapies and AZ1 presented in this manuscript.

1259

1260

1261

1262

1263

1264

1265

1266

1267

1268

1269

1270

1271

1272

1273

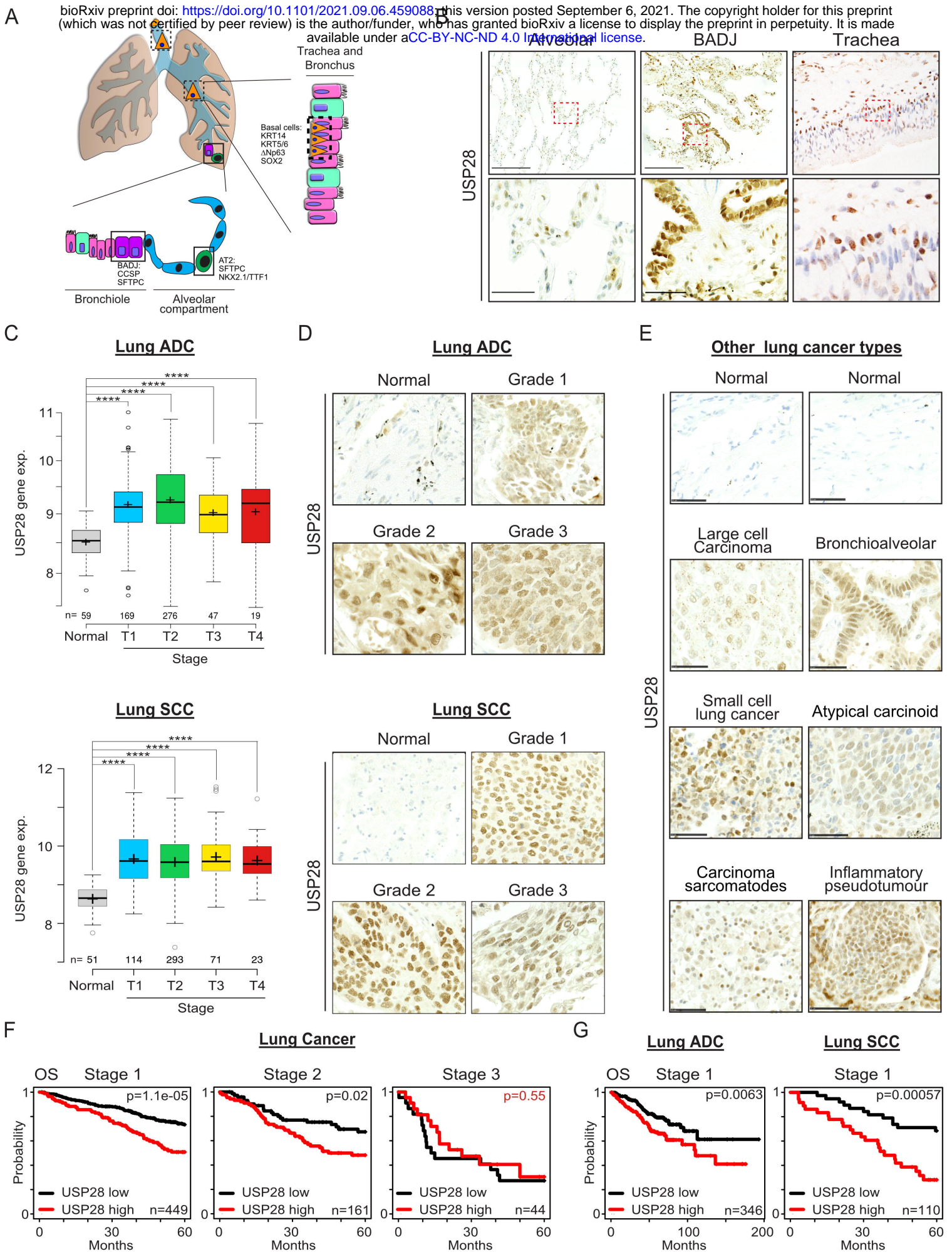
1274

1275

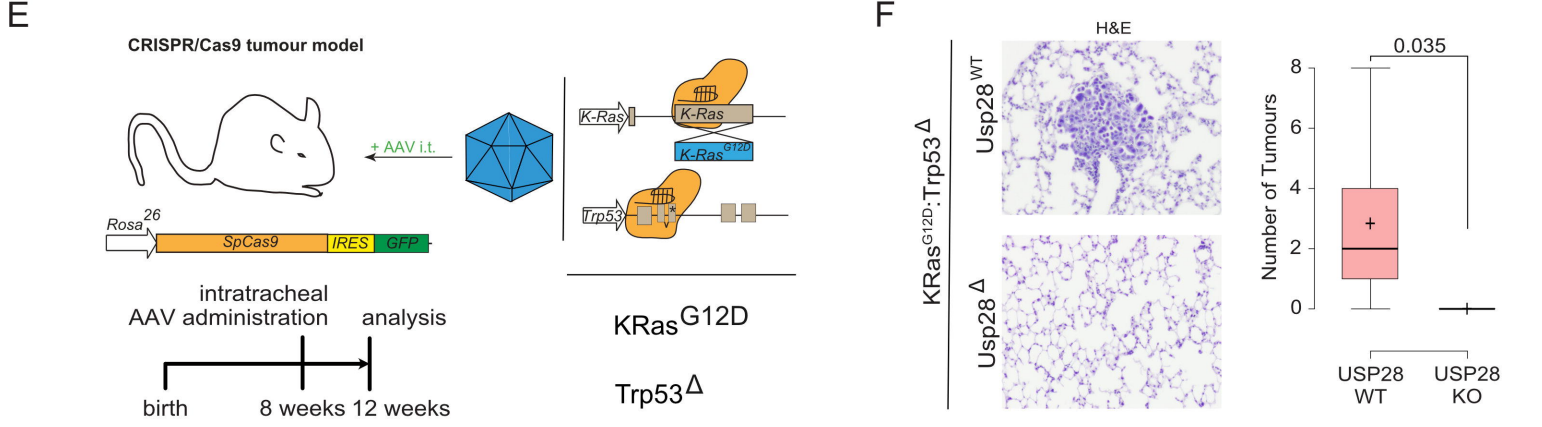
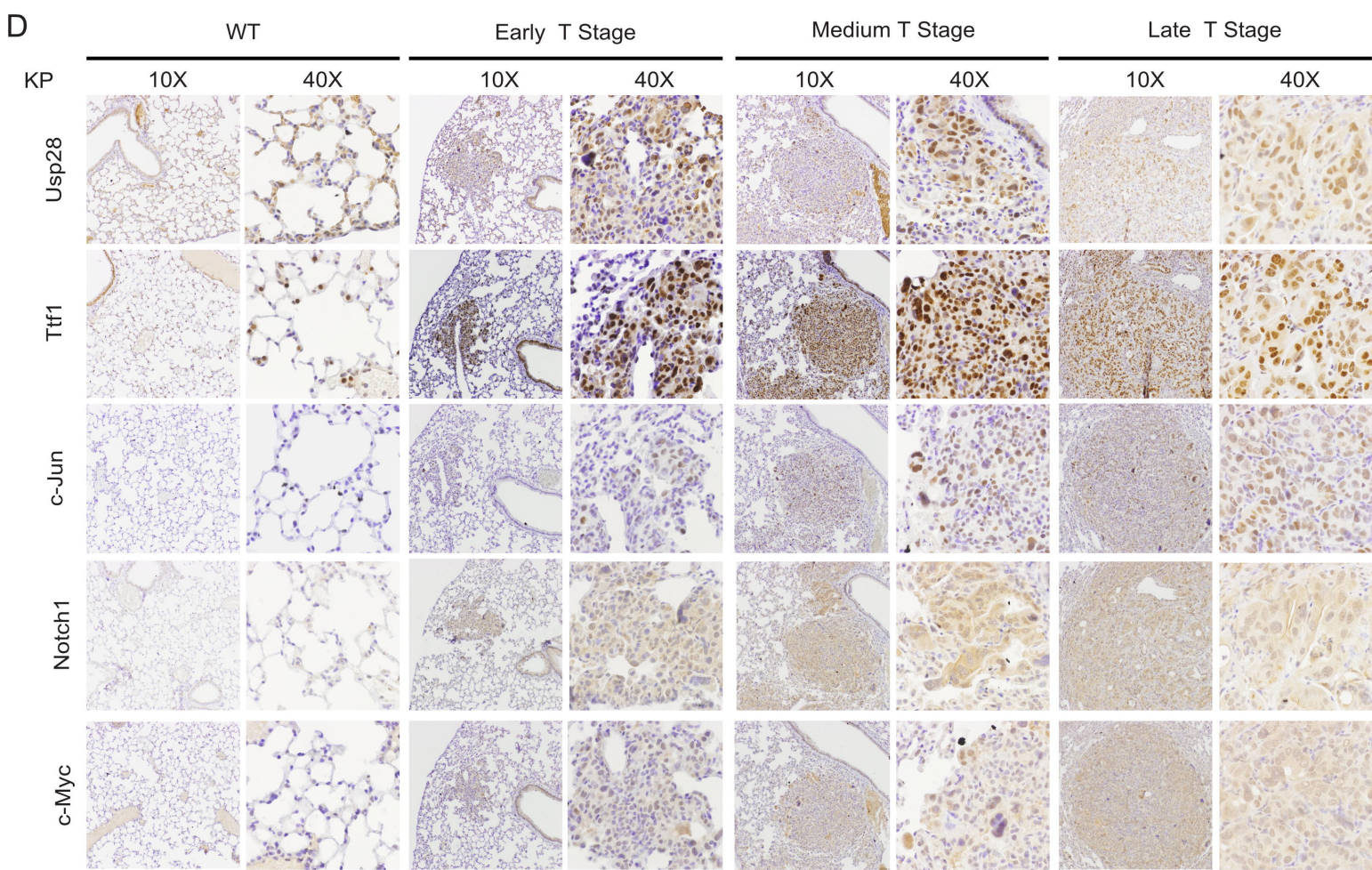
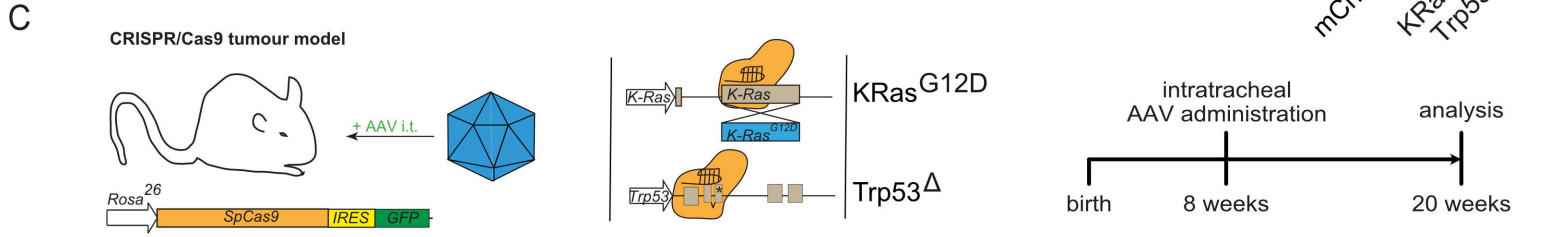
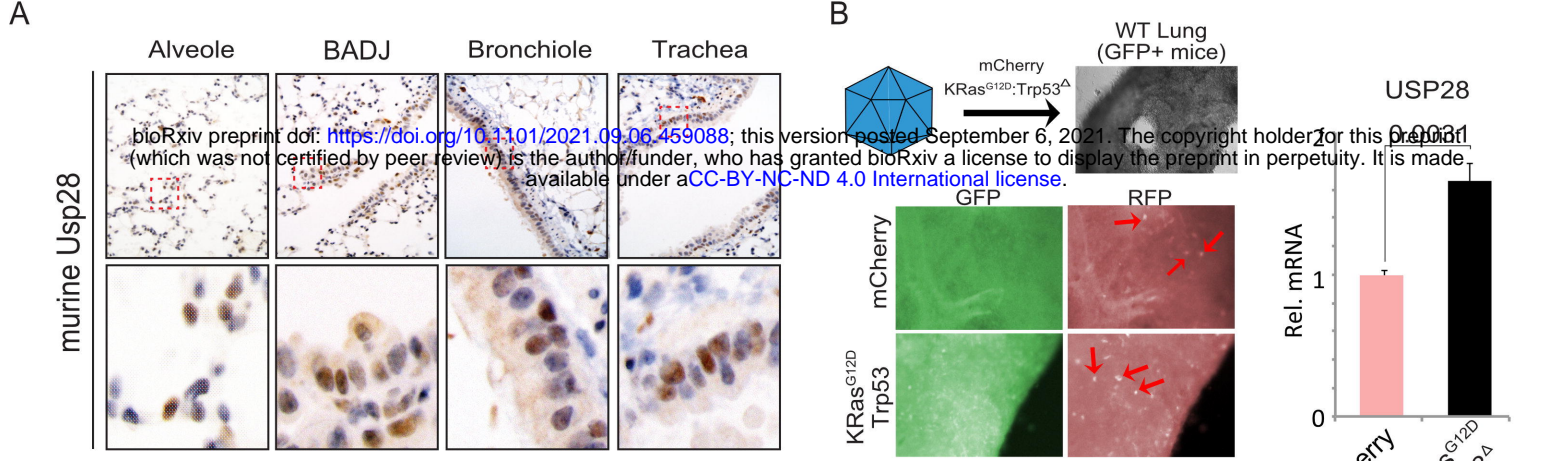
1276

1277

1278  
1279  
1280  
1281  
1282  
1283  
1284  
1285  
1286  
1287  
1288  
1289  
1290  
1291  
1292



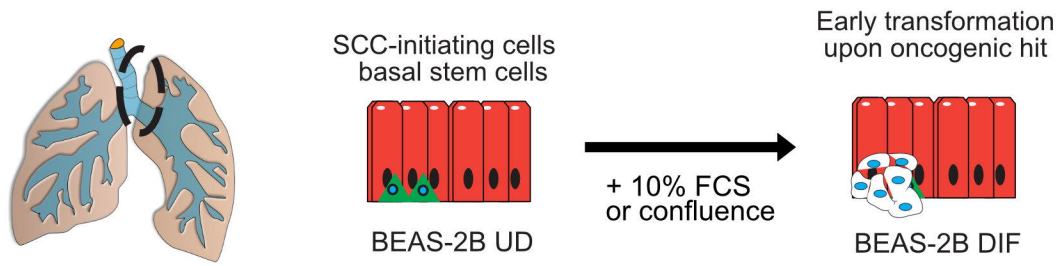




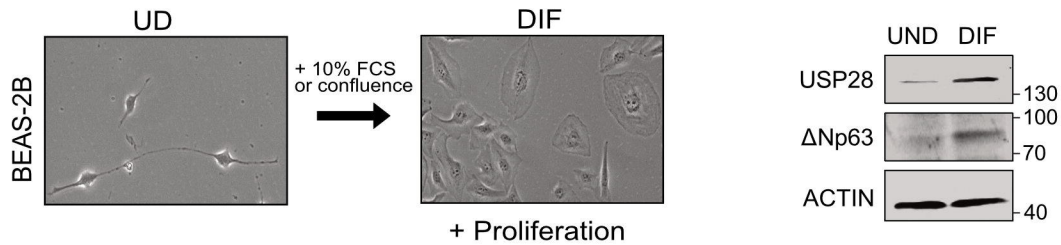
Prieto-Garcia et al. Figure 2



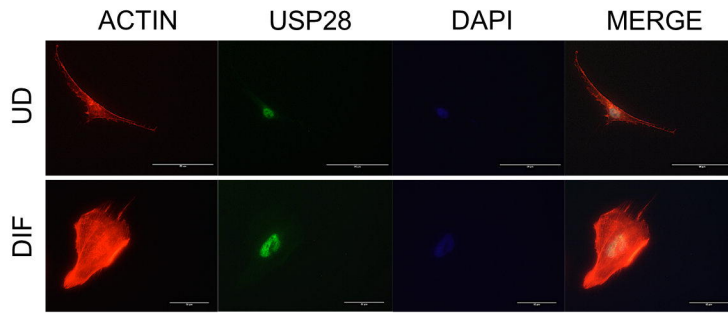
A



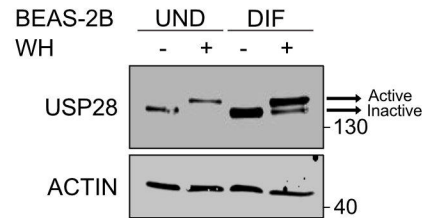
B



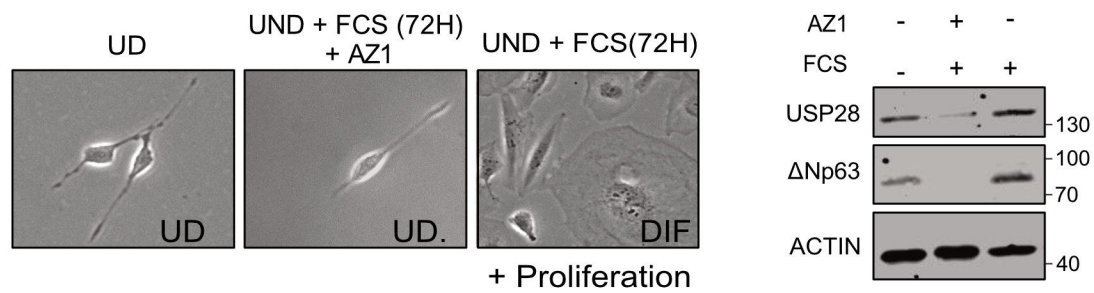
C



D

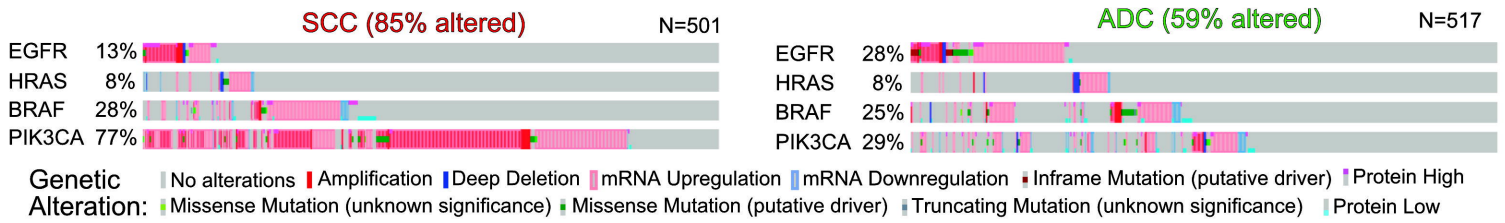


E

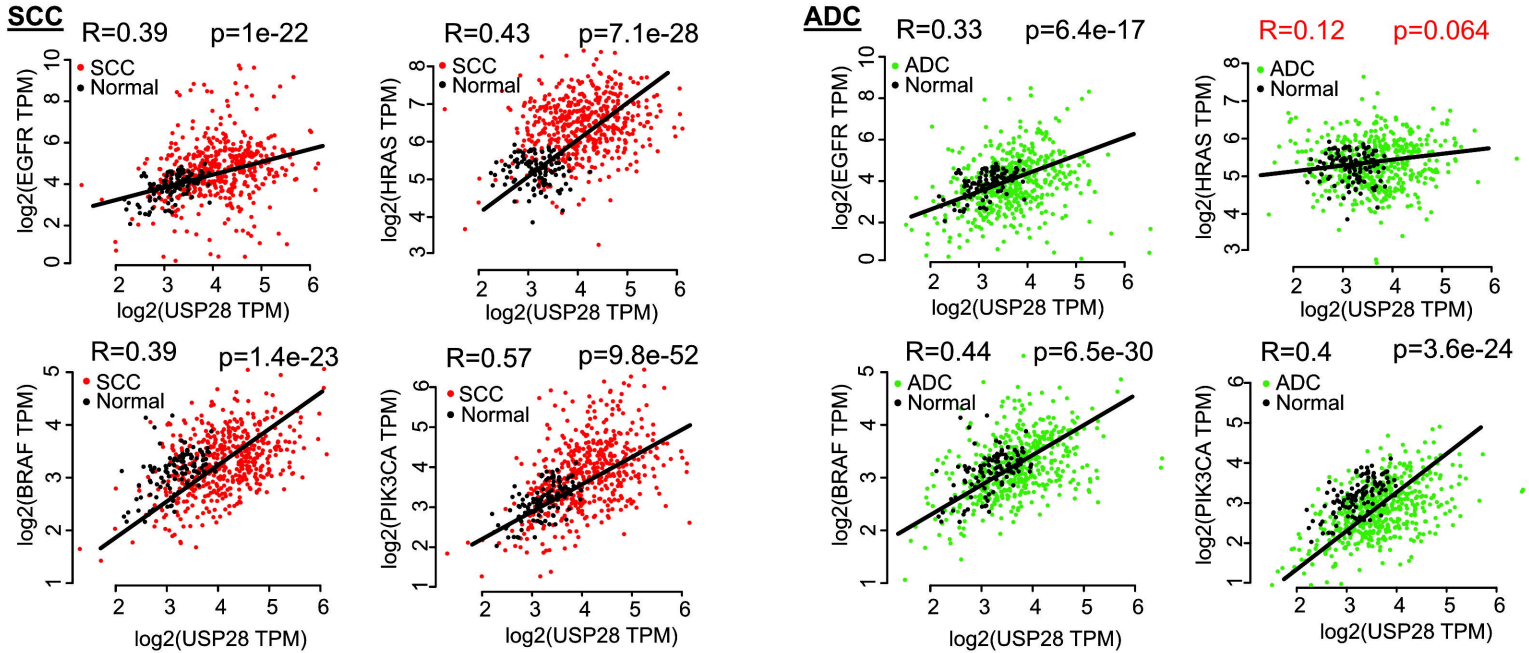




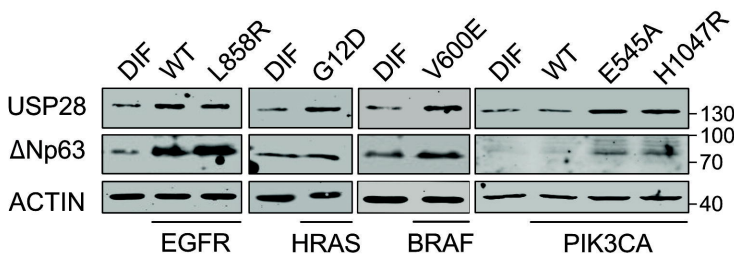
A



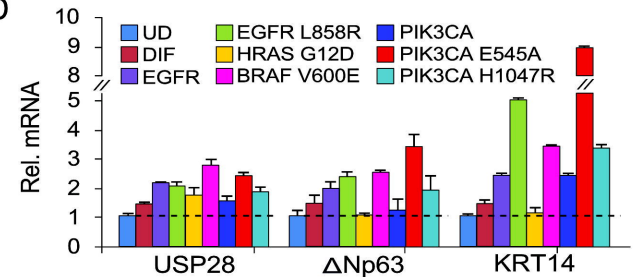
B



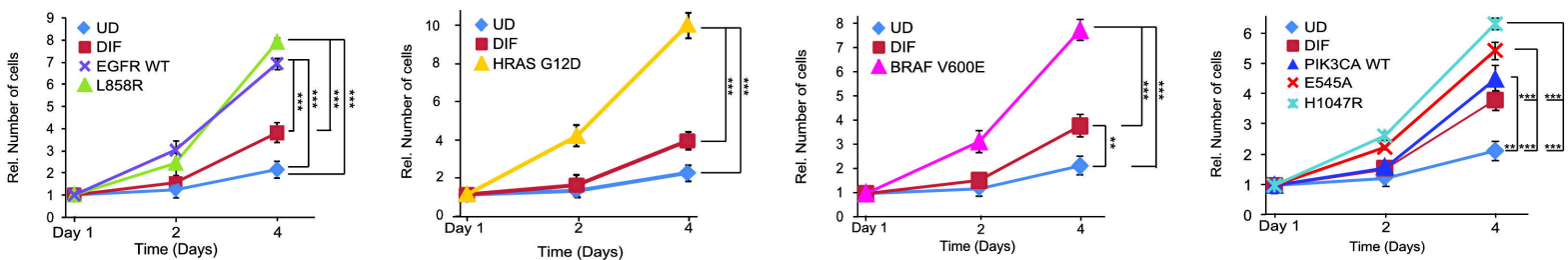
C



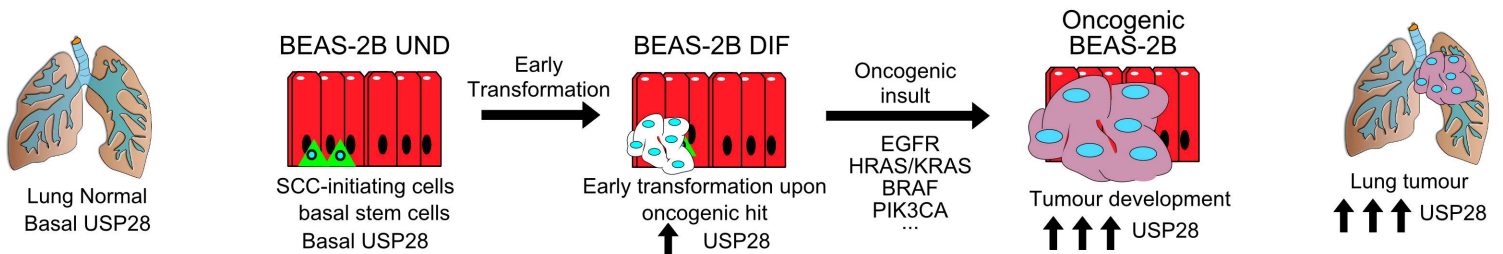
D

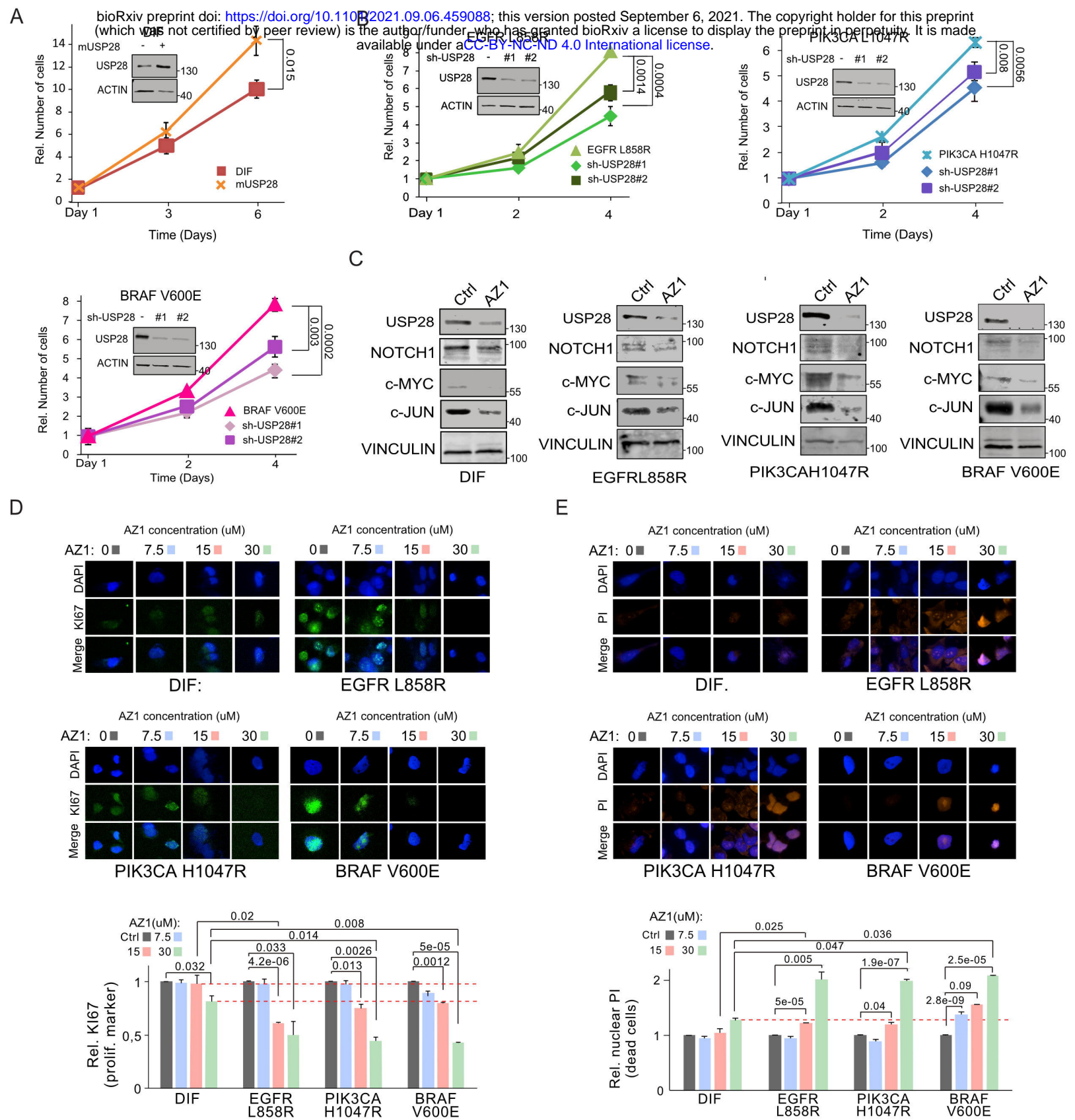


E

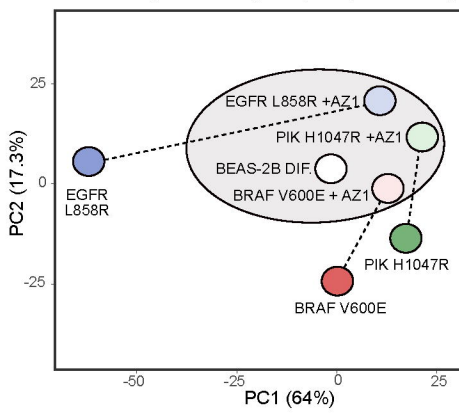


F



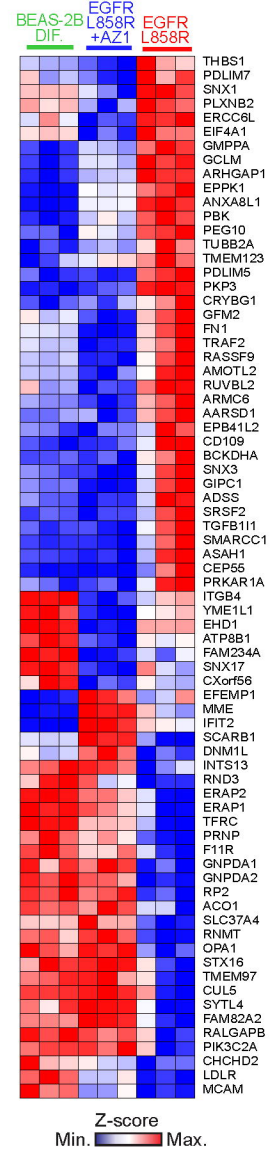
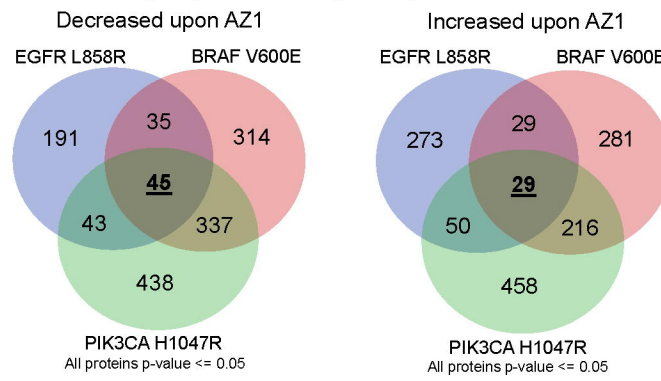


A

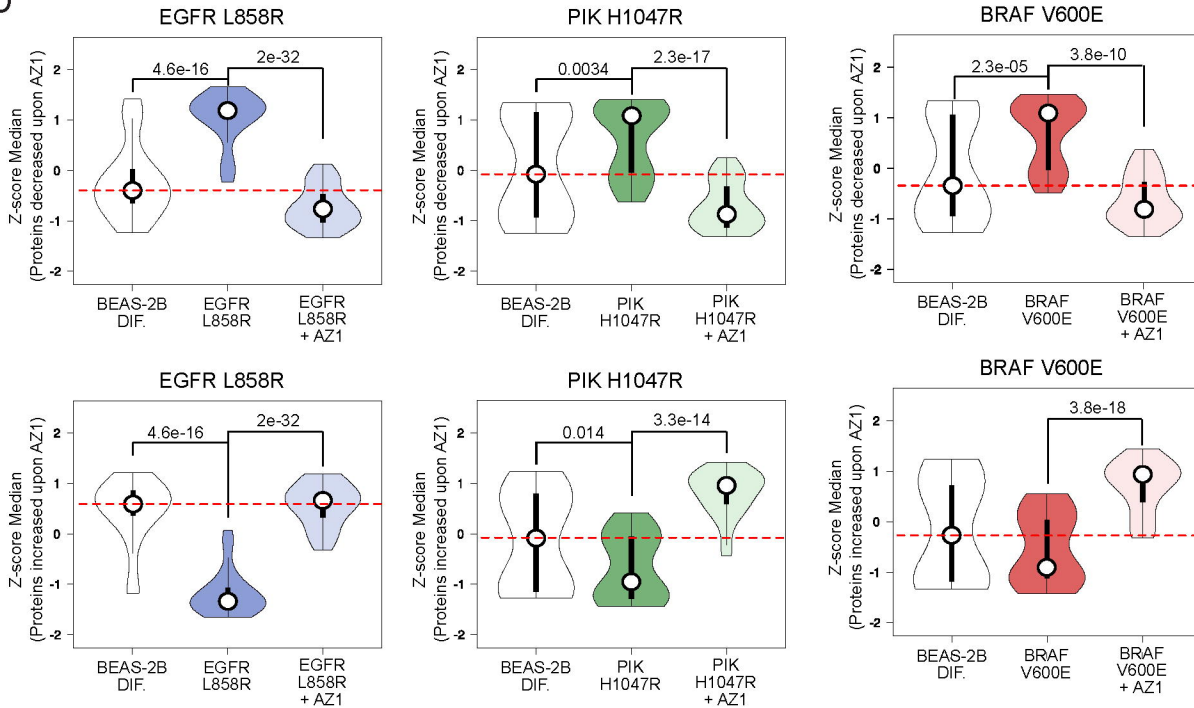


B

Proteins dysregulated during oncogenic transformation

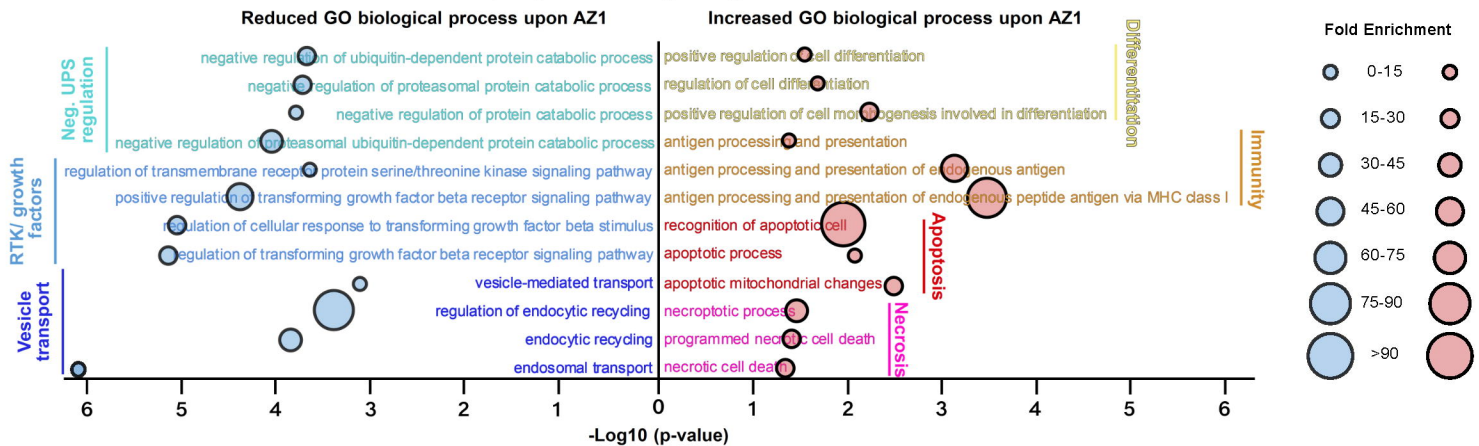


D

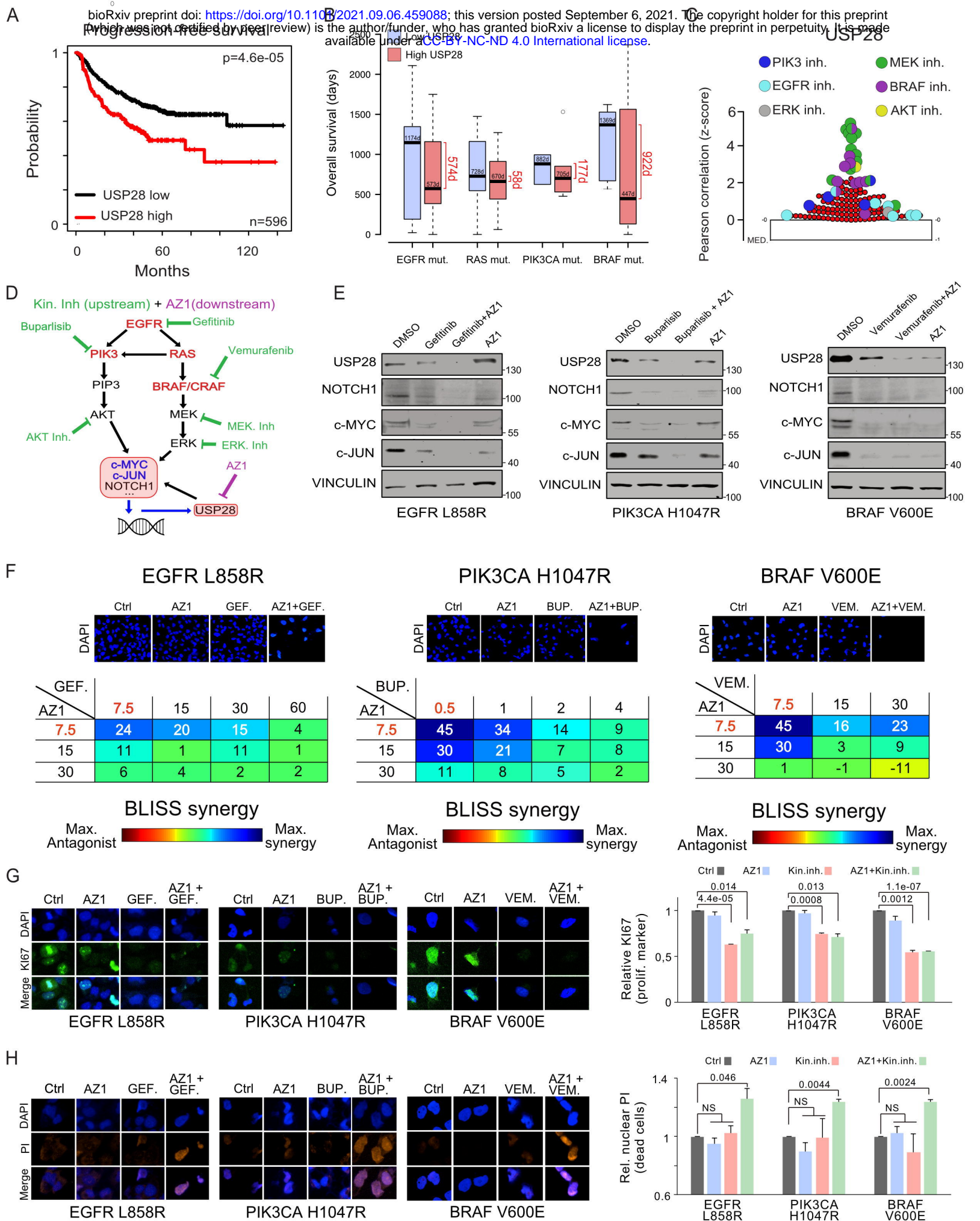


E

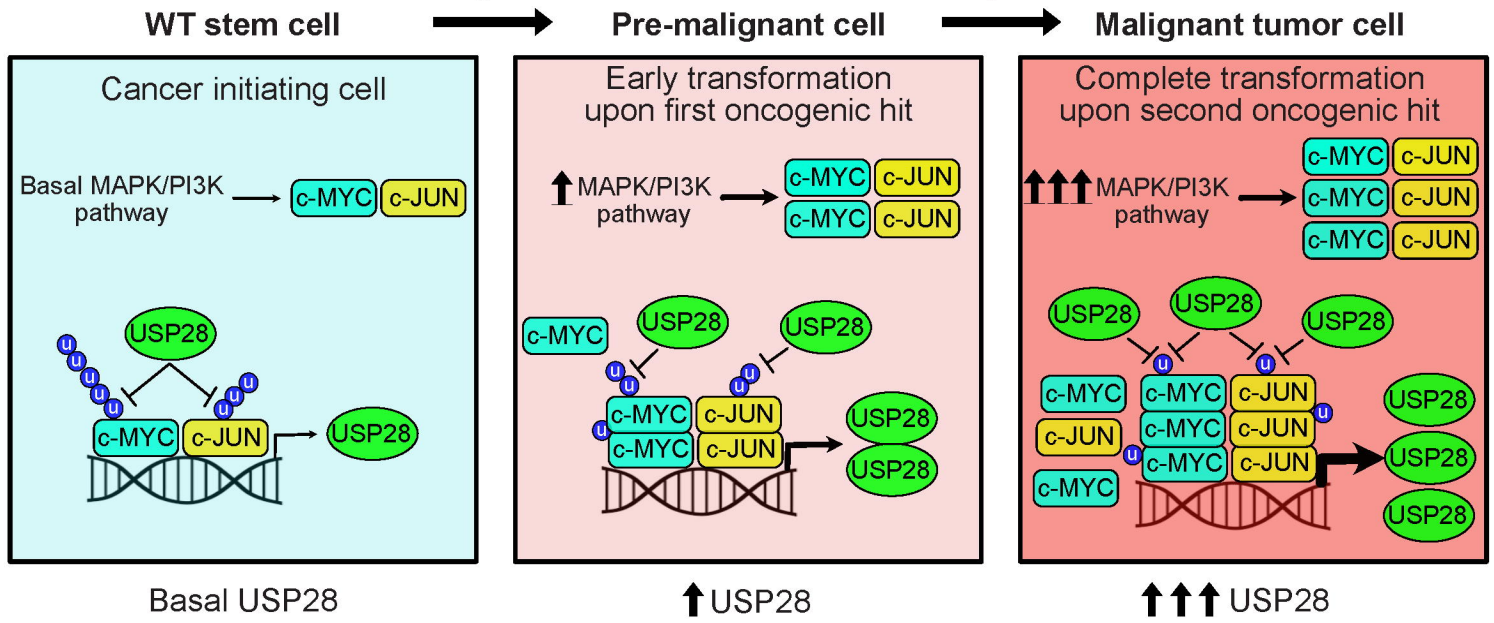
Proteins dysregulated during oncogenic transformation







A



B

